

Activation of HER3 Interferes with Antitumor Effects of Axl Receptor Tyrosine Kinase Inhibitors: Suggestion of Combination Therapy¹

Robert Torka^{*,2}, Kinga Péntes^{*,5,2},
Simone Gusenbauer^{*}, Christine Baumann^{*},
István Szabadkai[†], László Örfi^{†,‡},
György Kéri^{†,5} and Axel Ullrich^{*}

*Department of Molecular Biology, Max Planck Institute of Biochemistry, Martinsried, Germany; [†]Vichem Chemie Research Ltd, Budapest, Hungary; [‡]Department of Pharmaceutical Chemistry, Semmelweis University, Budapest, Hungary; [§]MTA-SE (Magyar Tudományos Akadémia -Semmelweis Egyetem) Pathobiochemistry Research Group, Department of Medical Chemistry, Semmelweis University, Budapest, Hungary

Abstract

The Axl receptor tyrosine kinase (RTK) has been established as a strong candidate for targeted therapy of cancer. However, the benefits of targeted therapies are limited due to acquired resistance and activation of alternative RTKs. Therefore, we asked if cancer cells are able to overcome targeted Axl therapies. Here, we demonstrate that inhibition of Axl by short interfering RNA or the tyrosine kinase inhibitor (TKI) BMS777607 induces the expression of human epidermal growth factor receptor 3 (HER3) and the neuregulin 1(NRG1)–dependent phosphorylation of HER3 in MDA-MB231 and Ovar8 cells. Moreover, analysis of 20 Axl-expressing cancer cell lines of different tissue origin indicates a low basal phosphorylation of RAC- α serine/threonine-protein kinase (AKT) as a general requirement for HER3 activation on Axl inhibition. Consequently, phosphorylation of AKT arises as an independent biomarker for Axl treatment. Additionally, we introduce phosphorylation of HER3 as an independent pharmacodynamic biomarker for monitoring of anti-Axl therapy response. Inhibition of cell viability by BMS777607 could be rescued by NRG1-dependent activation of HER3, suggesting an escape mechanism by tumor microenvironment. The Axl-TKI MPCD84111 simultaneously blocked Axl and HER2/3 signaling and thereby prohibited HER3 feedback activation. Furthermore, dual inhibition of Axl and HER2/3 using BMS777607 and lapatinib led to a significant inhibition of cell viability in Axl-expressing MDA-MB231 and Ovar8 cells. Therefore, we conclude that, in patient cohorts with expression of Axl and low basal activity of AKT, a combined inhibition of Axl and HER2/3 kinase would be beneficial to overcome acquired resistance to Axl-targeted therapies.

Neoplasia (2014) 16, 301–318

Introduction

Axl is a member of the unique Tyro3, Axl, MerTK family of receptor tyrosine kinases (RTKs). *Axl* was first identified as an oncogene in patients with chronic myelogenous leukemia [1] and was shown to have transforming activity when transfected into NIH/3T3 cells [2]. Axl activation occurs by binding of *growth arrest–specific gene 6*, its only validated ligand [3,4]. Axl signaling stimulates phosphatidylinositol 3-kinase/RAC- α serine/threonine-protein kinase (PI3K/AKT), extracellular signal-regulated kinase (ERK) and p38 mitogen-activated protein kinase cascades, the nuclear factor-kappa B (NF- κ B) pathway, and signal transducer and activator of transcription signaling [5]. Consequently, Axl signaling modulates biologic

processes, including invasion, angiogenesis, resistance to chemotherapeutics and targeted drugs, survival, and proliferation, which represent characteristics associated with malignancies [6].

Address all correspondence to: Robert Torka, PhD, Department of Molecular Biology, Max Planck Institute of Biochemistry, Am Klopferspitz 18, D-85152, Martinsried, Germany. E-mail: torka@biochem.mpg.de

¹This work was supported by Max Planck Society. Conflict of interest: The authors declare no conflict of interest.

²These authors contributed equally to this work.

Received 14 February 2014; Revised 10 March 2014; Accepted 11 March 2014

Copyright © 2014 Neoplasia Press, Inc. All rights reserved 1476-5586/14
<http://dx.doi.org/10.1016/j.neo.2014.03.009>

Subsequent to its original discovery in patients with chronic myelogenous leukemia, Axl expression was observed in more than 20 human tumor entities and is associated in most cases with tumor progression [7]. High expression of Axl in primary lung and pancreatic adenocarcinomas correlates with lymph node status and disseminated disease [8–10]. In glioblastoma multiforme, Axl expression is associated with an actively migrating cell population that predicts aggressive behavior [11]. Importantly, primary ovary carcinoma [12], lung carcinoma [13], breast carcinoma [14], renal cell carcinoma [15], glioblastoma multiforme [16], or acute myeloid leukemia [17] with high Axl expression levels correlate with shorter progression-free and overall survival. These studies suggest that expression of Axl confers aggressive tumor behavior, leading to tumor dissemination and mortality from metastasis.

Axl up-regulation has also been described in cisplatin-resistant ovarian cancer [18], doxorubicin-resistant acute myeloid leukemia [19], lapatinib-resistant breast cancer [20], imatinib-resistant gastrointestinal stromal tumors [21], and imatinib-resistant chronic myeloid leukemia [22]. Lately, Axl activation has been reported as a cause of resistance to epidermal growth factor receptor (EGFR)-targeted therapy in non-small cell lung cancers [23,13]. These studies support the well-known fact that the benefits of single-targeted therapies are limited due to resistance formation by activation of alternative RTKs. Hence, we asked if targeted Axl therapies would result in the activation of other RTKs to circumvent Axl inhibition. To answer this question, we blocked Axl phosphorylation in MDA-MB231 cells overexpressing Axl by short interfering RNA-mediated knockdown or by treatment with three selective Axl tyrosine kinase inhibitors (TKIs), namely, BMS777607, R428, and MPCD84111. BMS777607 was recently published as a Met inhibitor but also targets Axl RTK very potently at low nanomolar concentrations [24]. R428 is a selective TKI published by Holland et al. entering clinical phase I studies in the near future [25]. MPCD84111 was recently patented as a new Axl TKI by our group.

In contrast to MPCD84111, BMS777607 and R428 induce a v-erb-b2 avian erythroblastic leukemia viral oncogene homolog 3/human epidermal growth factor receptor 3 (ERBB3/HER3)-activating feedback loop mechanism depending on inhibition of PI3K/AKT signaling. Inhibition of cell viability by BMS777607 was rescued with the HER2/3 ligand neuregulin 1 (NRG1), suggesting a possible mechanism of tumor cell escape. MPCD84111 simultaneously blocked Axl and HER2/3 signaling, thereby prohibiting this HER3 feedback loop. Importantly, blocking of Axl by BMS777607 and HER2/3 by lapatinib led to synergistic or at least additive inhibition of cell viability of MDA-MB231 and Ovar8 cells. This provides a strong rationale for combined inhibition of Axl and HER2/3 kinase signaling in patients with Axl-amplified tumors.

Materials and Methods

Cell Culture Techniques

Cell lines were grown in a humidified, 5% CO₂ incubator at 37°C. The human cancer cell lines MDA-MB231, A549, C4-I, A172, U373, Panc-1, SF126, U118, and NIH/3T3-Axl fibroblasts were maintained in Dulbecco's modified Eagle medium supplemented with 1% sodium pyruvate and 10% FBS. Hs578T, NCI-H1975, NCI-H1299, NCI-H292, Ovar8, BxPC3, BT549, MDA-MB436, and MDA-MB468 were routinely passaged in Roswell Park

Memorial Institute 1640 medium supplemented with 1% glutamine and 10% FBS. MDA-MB231-D3H2LN and Capan-2 were cultivated in minimum essential media supplemented with 1% sodium pyruvate, 1% glutamine, 1% nonessential amino acids, and 10% FBS. McCoy 5A medium (modified) supplemented with 10% FBS was used for SKOV-3 cells. Cell culture media were purchased from Gibco (Invitrogen, Bleiswijk, The Netherlands), and supplements were ordered from GE Healthcare (Wien, Austria).

Three dimensional (3D) Spheroid Culture

BD Matrigel Basement Membrane Matrix (BD Biosciences, Bedford, MA, No. 354234) was diluted at a concentration of 3 mg/ml in cell line–corresponding serum-free medium. Eighty microliters of precooled Matrigel was pipetted into the wells of precooled 96-well plates. The Matrigel polymerized at least 16 hours at 37°C. Cells (7000 per well) in 120 µl of medium were seeded on top of the solid Matrigel and formed spheroidlike structures within 72 hours. Inhibitor treatments were initiated at the moment of cell seeding into Matrigel.

RNA Interference

Transfection of 21-nucleotide siRNA duplexes (Axl No. s1845, Met No. s8701, HER2 No. 540, HER3 No. s4780, and Ambion Control No. 1; Ambion/Invitrogen, Darmstadt, Germany and EGFR, No. J-003114-13; Thermo Scientific Dharmacon, Schwerte, Germany) was carried out using Lipofectamine RNAiMAX (Invitrogen, Darmstadt, Germany) and OPTI-MEM media (Gibco/Invitrogen, Bleiswijk, The Netherlands). After 6 hours, medium was changed to normal medium containing 10% FBS. Cells were used for subsequent experiments after additional 48 hours of incubation.

Cell Viability

We measured cell viability using a luciferase-coupled ATP quantitation assay (CellTiter-Glo; Promega, Mannheim, Germany). Cells were incubated for 72 hours, and the CellTiter-Glo reagent was added according to the manufacturer's instructions. The luminescence signal was recorded using a microplate luminometer, LB 96V (Berthold Technologies, Bad Wildbad, Germany). The experiments were performed at least in triplicate.

Human Phospho-RTK Array

Human Phospho-RTK array (R&D Systems GmbH, Wiesbaden-Nordenstadt, Germany, No. ARY001) was used according to the manufacturer's instructions. Briefly, cells were lysed on ice in lysis buffer [50 mM Hepes (pH 7.5), 150 mM NaCl, 1 mM EGTA, 10% glycerol, 1% Triton X-100, 100 mM NaF, 10 mM Na₄P₂O₇·10 H₂O, 1 mM Na₃VO₄, 1 mM PMSF, and 10 mg/ml aprotinin, all purchased from Sigma-Aldrich, Steinheim, Germany] for 15 minutes. Five hundred micrograms of lysates was incubated with blocked array membranes overnight. Detection was performed using enhanced chemiluminescence (Western Lightning; PerkinElmer, Rodgau, Germany).

Western Blot Analysis

Cells were lysed in lysis buffer for 15 minutes. Equal amounts of protein were resolved by sodium dodecyl sulfate–polyacrylamide gel electrophoresis. Proteins were transferred to nitrocellulose membranes (Schleicher and Schuell BioScience GmbH, Dassel, Germany), blocked for 1 hour, and incubated at 4°C overnight with the corresponding primary antibody. pHER3 Y1289 (No. 4791), pHER2 Y1248 (No. 2247), EGFR (No. 2232), and pAKT S473

(No. 9271) antibodies were purchased from Cell Signaling Technology (Cell Signaling Technology/New England Biolabs GmbH, Frankfurt am Main, Germany). The anti-HER2 (No. 06-562) and anti-HER3 (No. 05-390; Millipore, Schwalbach, Germany), anti-Met (No. sc-161; Santa Cruz Biotechnology, Heidelberg, Germany), and the anti-Tubulin (No. T9026) antibody was purchased from Sigma-Aldrich. For phospho-tyrosine (p-Tyr) detection, the homemade anti-p-Tyr clone 4G10 was used. Membranes were blocked and incubated with an HRP-conjugated anti-rabbit or anti-mouse secondary antibody (Jackson Immuno Research Europe Ltd., Suffolk, UK) for 1 hour at room temperature. Detection was performed using enhanced chemiluminescence (Western Lightning; PerkinElmer, Rodgau, Germany). Densitometric analysis was conducted using ImageJ software from the National Institutes of Health (Bethesda, MD). The changes of intensity reported in the figures were obtained as a ratio between the DMSO control or siRNA control band intensity and the band intensity of interest after indicated treatment. All bands were normalized to Tubulin as loading control.

Immunoprecipitation

Respective antibodies were precoupled to 40 μ l of A-Sepharose beads (GE Healthcare, Munich, Germany, No. 17-5280-04) in lysis buffer for 1 hour and washed three times with lysis buffer. Lysates and precoupled antibody-beads were incubated at 4°C for 16 hours, and precipitates were washed three times with 1 ml of lysis buffer, suspended in Laemmli buffer, boiled for 10 minutes, and analyzed by Western blot. Antibodies used for immunoprecipitation (IP) were HER3 (No. 05-390) and HER2 (No. 06-562) purchased from Millipore or HER2 homemade antibody clone 13D1B1.

Enzyme-Linked Immunosorbent Assay (ELISA)

Phospho-Axl ELISA. Axl phosphorylation was determined using phospho-tyrosine Axl ELISA (p-Tyr-Axl ELISA). Onto six-well plates, 75,000 NIH/3T3-Axl cells were seeded, starved for 24 hours, and then treated with serially diluted inhibitor concentrations for 1 hour. Cells were lysed on ice in 400 μ l of lysis buffer for 15 minutes. Ninety-six-well Nunc MicroWell plates (Fisher Scientific GmbH, Schwerte, Germany) were coated overnight with 2 μ g/ml homemade anti-Axl capture antibody (homemade clone 259/2, IgG1 isotype) in phosphate-buffered saline (PBS) (100 μ l per well). Subsequently, 96-well plates were blocked with PBS/0.05% Tween 20 (Sigma-Aldrich, Steinheim, Germany) + 10% FBS for 4 hours at 37°C. Plates were washed five times with PBS/0.05% Tween 20, and 95 μ l of lysate was transferred per well for incubation overnight at 4°C. Plates were washed five times with PBS/0.05% Tween 20. For detection of phosphorylated tyrosine, we used the biotinylated homemade anti-p-Tyr clone 4G10 antibody (0.5 μ g/ml) in PBS/0.05% Tween 20 + 10% FBS (100 μ l per well) and incubated the 96-well plate for 2 hours at room temperature. The 4G10 antibody was biotinylated with Sulfo-NHS-Biotin according to the supplier's protocol (Pierce, Rockford, IL) and purified by Micro Bio-Spin 6 chromatography columns (Bio-Rad Laboratories, Inc, Hercules, CA) using PBS as diluent. Plates were washed five times with PBS/0.05% Tween 20. Alkaline phosphatase-conjugated streptavidin SA110 (Millipore, Schwalbach, Germany) (1:4000) was used in PBS/0.05% Tween 20 + 10% FBS (100 μ l per well) and incubated for 30 minutes at room temperature. Plates were washed five times with PBS/0.05% Tween 20. For fluorometric detection of alkaline phosphatase,

AttoPhos substrate set (Roche Diagnostics GmbH, Mannheim, Germany) was used (100 μ l per well). The fluorometric signal was quantified after 90 minutes at a wavelength of 430/560 nm using a TECAN Ultra Evolution plate reader (Tecan Deutschland GmbH, Crailsheim, Germany). The Patent No. WO2011045084A owned by the Max Planck Society contains a detailed description of the p-Tyr-Axl ELISA and the generation of Axl-expressing NIH/3T3-Axl cells used for this ELISA.

Neuregulin 1-enzyme-linked immunosorbent assay. We used a specific human NRG1-ELISA (R&D Systems GmbH, Wiesbaden-Nordenstadt, Germany, No. DY377) to quantify protein amounts according to the manufacturer's protocol with the following modifications: After the incubation with a biotinylated detection antibody specific for NRG1 (1:180), we used an alkaline phosphatase-conjugated streptavidin SA110 (Millipore, Schwalbach, Germany) (1:4000) at room temperature. For fluorometric detection of alkaline phosphatase, AttoPhos substrate set (Roche Diagnostics GmbH, Mannheim, Germany) was used (100 μ l per well). The fluorometric signal was quantified after 90 minutes at a wavelength of 430/560 nm using a TECAN Ultra Evolution plate reader (Tecan Deutschland GmbH, Crailsheim, Germany). All antibodies were diluted in PBS/0.05% Tween 20 + 1% BSA (100 μ l per well). The plates were washed five times with PBS/0.05% Tween 20.

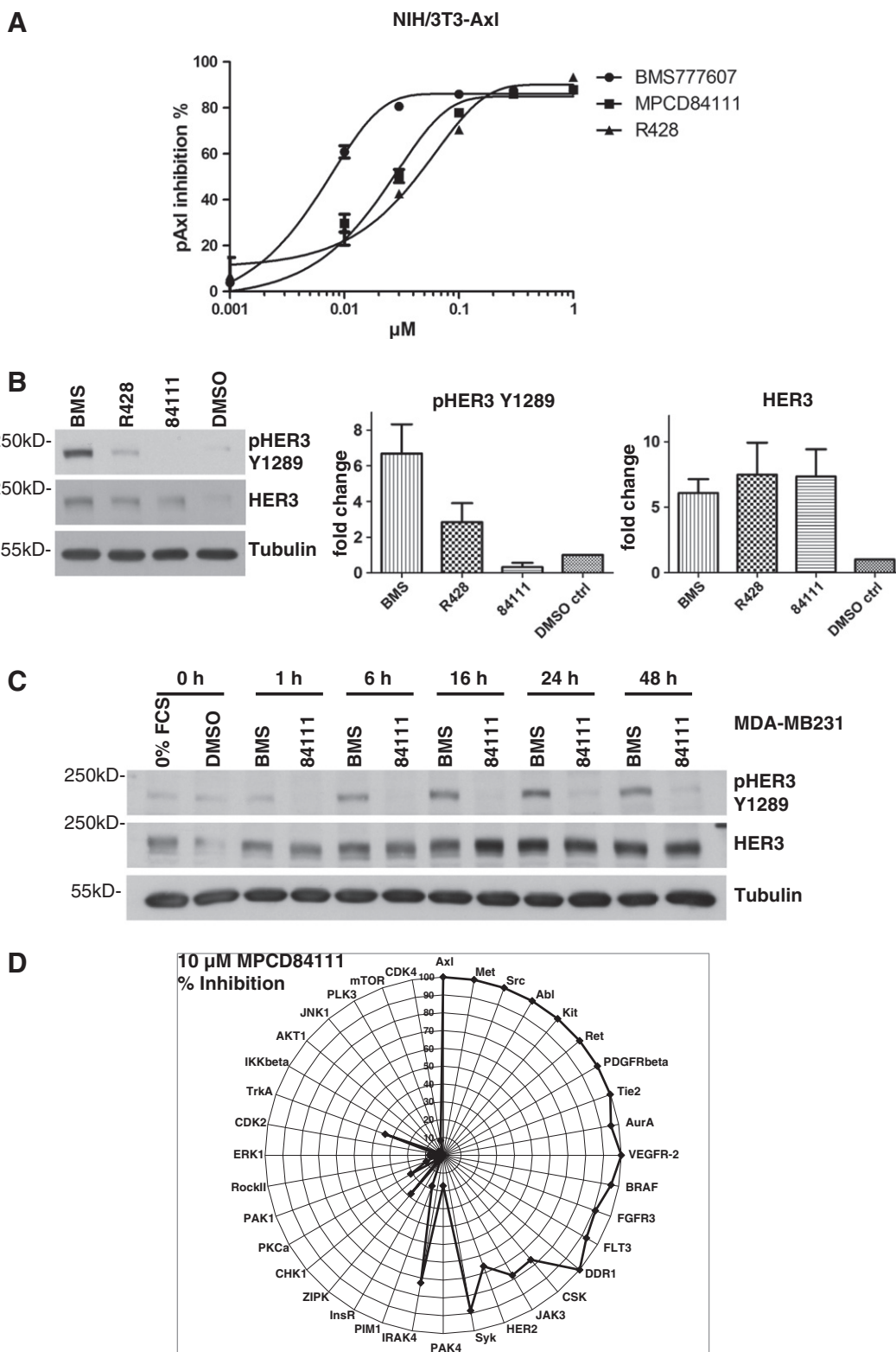
Phospho-AKT S473 ELISA. The Pan AKT-specific ELISA kit (R&D Systems GmbH, Wiesbaden-Nordenstadt, Germany, No. DYC887B-5) was used for quantification of phospho-AKT S473 according to the manufacturer's protocol with the following modifications: After the incubation with a biotinylated phospho-AKT (S473) panspecific detection antibody (1:180), we used an alkaline phosphatase-conjugated streptavidin SA110 (Millipore, Schwalbach, Germany) (1:4000) at room temperature. For fluorometric detection of alkaline phosphatase, AttoPhos substrate set (Roche Diagnostics GmbH, Mannheim, Germany) was used (100 μ l per well). The fluorometric signal was quantified after 90 minutes at a wavelength of 430/560 nm using a TECAN Ultra Evolution plate reader (Tecan Deutschland GmbH, Crailsheim, Germany). All antibodies were diluted in PBS/0.05% Tween 20 + 1% BSA (100 μ l per well). The plates were washed five times with PBS/0.05% Tween 20.

Quantitative Polymerase Chain Reaction

MDA-MB231 cells were treated with 10 μ M BMS777607 or DMSO for the indicated periods of time. RNA preparation [RNeasy Mini Kit (50); QIAshredder; Qiagen, Hilden, Germany] and first-strand cDNA synthesis (First Strand cDNA Synthesis Kit; Fermentas/Fisher Scientific GmbH) were performed according to the manufacturer's protocol. For cDNA synthesis, 1 μ g of total RNA and 200 ng of random hexamer primer were used. The Gene database search on National Center for Biotechnology Information platform (Bethesda, MD) revealed 17 different NRG1 isoforms in *Homo sapiens* (Gene ID: 3084): No. 1, NM_001159995.1; No. 2, NM_001159996.1; No. 3, NM_001159999.1; No. 4, NM_001160001.1; No. 5, NM_001160002.1; No. 6, NM_001160004.1; No. 7, NM_001160005.1; No. 8, NM_001160007.1; No. 9, NM_001160008.1; No. 10, NM_004495.3; No. 11, NM_013956.3; No. 12, NM_013957.3; No. 13, NM_013958.3; No. 14, NM_013959.3; No. 15, NM_013960.3; No. 16, NM_013962.2; and No. 17,

NM_013964.3. For HER3 (*ERBB3 v-erb-b2 avian erythroblastic leukemia viral oncogene homolog 3*; Gene ID: 2065), two different isoforms are described: No. 1, NM_001982.3 and No. 2, NM_001005915.1. Primers were designed to cover most of the 17 isoforms of NRG1. For cDNA quantitation, one sixtieth of the reverse transcriptase reaction was mixed with 0.5 μM gene-specific primers. Primers were given as follows: NRG1 primer set 1 (binding all isoforms

except Isoforms No. 2 and No. 14)—5'- TTCGCATTAACAAAG-CATCACTGG-3' (forward) and 5'- ATCTCGAGGGGT TTGAAAGGTCTT-3' (reverse); NRG1 primer set 2 (binding to isoform No. 2, No. 15 and No. 17)—5'- ACCTTTCAAACCCCTC-GAGATAC-3' (forward) and 5'- TCATGGGCACATTCTCAGTA-CAT-3' (reverse); and HER3 (binding only isoform No. 1)—5'- TGTGTAGCCAGCTGTCCCATAAC-3' (forward) and 5'-



GAGCCCGGTGATCAGAAAGTCC-3' (reverse); reference gene *HPRT1*-5'- GCTATAAATCTTTGCTGACCTGCTG-3' (forward) and 5' AATTACTTTTATGTCCCTGTTGACTGG-3' (reverse) and Fast SYBR Green Master Mix (Applied Biosystems) to a total volume of 12 μ l. The polymerase chain reaction (PCR) was carried out on a StepOnePlus instrument (Applied Biosystems, Darmstadt, Germany), according to the manufacturer's instruction.

Kinase Selectivity Profiling

The kinase selectivity profiling was performed by Proterus biostructures GmbH (Martinsried, Germany) according to the company's standard operation procedure. The calculations of percentage of inhibition have been performed using three different types of assays, namely, IMAP (Molecular Devices, Sunnyvale, CA), binding, and HTRF assays (Molecular Devices, Sunnyvale, CA). The radar blot in Figure 1D contains the data for the selectivity screening of compound MPCD84111 against 36 protein kinases normalized to a maximal inhibition of 100%. The experiments have been performed in triplicate.

IMAP assay. The IMAP assay (Molecular Devices, Sunnyvale, CA) detects kinase activity in solution. A fluorescently labeled substrate peptide is phosphorylated in the kinase reaction. After the reaction, a binding solution containing large trivalent metal-based nanoparticles is added, and the phosphorylated substrate binds to these beads. This reduces the rotational speed of the substrate, which can be detected using fluorescence polarization. The following kinases were used as substrates: Abl, AKT1, AurA, Axl, Cyclin-dependent kinase 2 (CDK2), CDK4, Serine/threonine-protein kinase Chk1/Checkpoint kinase-1 (CHK1), Kit, Met, Tyrosine-protein kinase CSK/C-Src kinase (CSK), Fibroblast growth factor receptor 3 (FGFR3), Receptor-type tyrosine-protein kinase FLT3/Fms-like tyrosine kinase 3 (FLT3), Inhibitor of nuclear factor kappa-B kinase subunit beta (IKK β), InsR, Interleukin-1 receptor-associated kinase 4 (IRAK4), Tyrosine-protein kinase JAK3/Janus kinase 3 (JAK3), Mitogen-activated protein kinase 8/c-Jun N-terminal kinase 1 (JNK1), Mitogen-activated protein kinase 3/Extracellular signal-regulated kinase 1 (ERK1), Serine/threonine-protein kinase PAK 1/p21-activated kinase 1 (PAK1), PAK4, Platelet-derived growth factor receptor beta (PDGFR β), Serine/threonine-protein kinase pim-1 (PIM1), Protein kinase C alpha type (PKC α), Serine/threonine-protein kinase PLK3/Polo-like kinase 3 (PLK3), Ret, RockII, Src, Syc, Tie2, TrkA, Vascular endothelial growth factor receptor 2 (VEGFR-2), and Death-associated protein kinase 3/Zipper-interacting protein kinase (ZIPK).

Binding assay. The binding assay is based on reporter probes that are designed to bind to the site of interest of the target protein. The binding of the reporter probe to the protein results in the emission of an

optical signal. Compounds that bind to the same site as the reporter probe displace the probe, causing signal diminution. Probe displacement is calculated in percentage. Signal reflecting 100% probe displacement is determined in the absence of enzyme, whereas 0% probe displacement is measured in the absence of compound. The reporter probe is used at a concentration reflecting its own K_d the equilibrium dissociation constant (probe) value. The following kinases were used as substrates: Serine/threonine-protein kinase B-raf/v-Raf murine sarcoma viral oncogene homolog B1 (BRAF), Epithelial discoidin domain-containing receptor 1 (DDR1), and Serine/threonine-protein kinase mTOR/Mammalian target of rapamycin (mTOR).

HTRF assay. This assay detects kinase activity with time-resolved fluorescence transfer (FRET). A biotinylated, kinase-specific peptide is phosphorylated in the kinase reaction. After the reaction, two detection reagents are added: first, an antibody recognizing the phosphorylated amino acid residue that is labeled with europium cryptate as a FRET donor and second, streptavidin that binds to the peptide through its biotin group and carries XL665 as a FRET acceptor. If the substrate becomes phosphorylated, the close proximity between the FRET donor and acceptor allows for the measurement of the time-resolved FRET signal. The HER2 kinase was analyzed by HTRF assay.

TKIs and Therapeutic Monoclonal Antibodies

Lapatinib and MPCD84111 were obtained from Vichem Chemie Research Ltd (Budapest, Hungary). MPCD84111 is patented under application example 12 from WO2011045084. BMS77607 and R428 were kind gifts from Lead Discovery Center GmbH (LDC, Dortmund, Germany). All inhibitors were dissolved in DMSO and stored at room temperature in 10 mM stock solution. The therapeutic monoclonal antibodies Herceptin and Erbitux were purchased from the Max Planck Pharmacy (Martinsried, Germany).

Ligands and Batimastat

The recombinant human NRG1 (No. 396-HB-050) and batimastat (BB94, No. 2961) were purchased from R&D Systems GmbH.

Microscopy

Phase-contrast images were captured on a Axiovert 300 microscope (Carl Zeiss, Jena, Germany) using MetaMorph (Molecular Devices, Sunnyvale, CA).

Statistical Data Analysis

All assays were performed at least in triplicate. Mean values and SEM are shown. Half maximal inhibitory concentration IC_{50} values

Figure 1. HER3 activation is a common feedback mechanism of Axl inhibitors, and MPCD84111 blocks phosphorylation of HER3 in contrast to BMS77607. (A) Inhibition of Axl phosphorylation was determined 1 hour posttreatment with BMS77607, MPCD84111, and R428 by p-Tyr-Axl ELISA in NIH/3T3-Axl cells. IC_{50} values were calculated by four-parameter log curve fit. Axl kinase activity was inhibited in a dose-dependent manner, with an IC_{50} value of 0.006 μ M for BMS77607, 0.027 μ M for MPCD84111, and 0.043 μ M for R428. (B) Axl Inhibitors induce HER3 expression. Western blot analysis of MDA-MB231 cells treated with 10 μ M BMS77607, MPCD84111, and R428 for 24 hours. BMS77607 and R428 caused an increase in pHER3 Y1289 after 24 hours of treatment in contrast to MPCD84111. Treatment with all three Axl inhibitors leads to a six- to 7.5-fold up-regulation of HER3 protein levels. The diagrams show the densitometric analysis of Western blots for pHER3 Y1289 and HER3. Mean values and SEM are shown ($n = 3$). (C) MPCD84111 blocks phosphorylation of HER3 in contrast to BMS77607. Western blot analysis of MDA-MB231 cells treated with 1 μ M BMS77607 or MPCD84111 up to 48 hours is shown. BMS77607 caused an increase in pHER3 Y1289 after 6 hours of treatment in contrast to MPCD84111. Both inhibitors induced a significant increase in protein expression of HER3 after 16 hours of treatment. (D) The kinase selectivity profile against a panel of 36 human kinases proves HER2 as a direct target of MPCD84111. The selectivity profiling was performed in triplicate at a compound concentration of 10 μ M. The plots indicate the percentages of inhibition for each individual kinase.

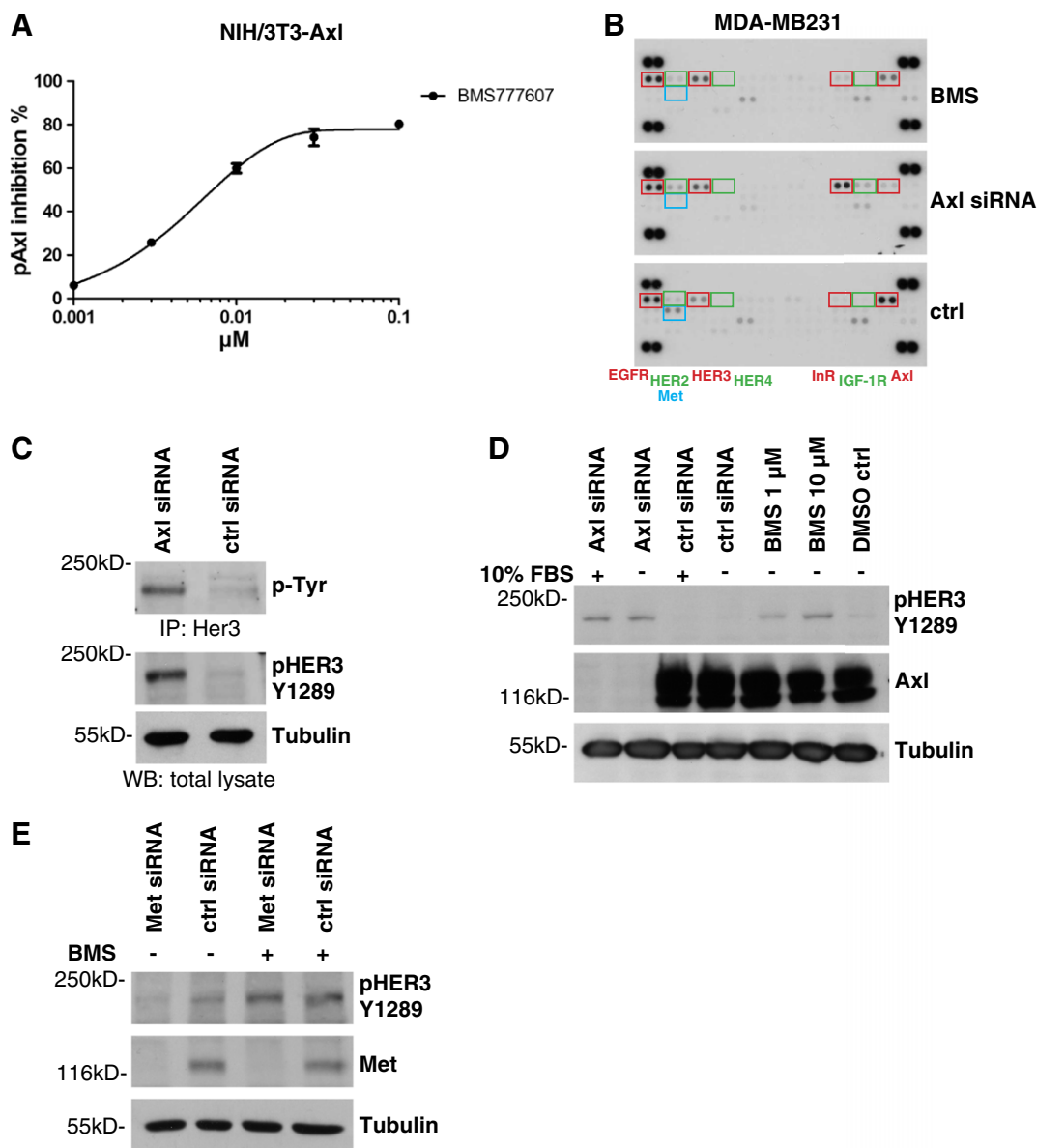


Figure 2. Inhibition of the Axl RTK leads to up-regulation of HER3 phosphorylation. (A) Inhibition of Axl phosphorylation was determined 1 hour posttreatment with BMS777607 by p-Tyr-Axl ELISA in NIH/3T3-Axl cells. IC₅₀ values were calculated by four-parameter log curve fit. (B) Axl inhibition led to an up-regulation of HER3 phosphorylation as determined by the Human Phospho-RTK Array Kit. MDA-MB231 cells were incubated with 1 μM BMS777607 for 24 hours or Axl-specific siRNA for 48 hours. The capture antibodies have been spotted in duplicates. The coordinates in the membrane for EGFR, HER2, Met, HER3, HER4, InR, IGF1R, and Axl are highlighted by rectangles. The corresponding antibody names are labeled at the bottom of the three displayed membranes from left to the right. (C) Validation of HER3 phosphorylation by HER3 immunoprecipitation with a HER3-specific antibody (Millipore, No. 05-390) and the Western blot for p-Tyr. The site-specific pHER3 Y1289 antibody displayed the same up-regulation of HER3 phosphorylation in Western blot experiments after treatment of MDA-MB231 cells with Axl-specific siRNA for 48 hours. Tubulin served as loading control. (D) Validation of HER3 phosphorylation by Western blot analysis of MDA-MB231 cells treated with Axl-specific siRNA for 48 hours or with 1 or 10 μM BMS777607 for 24 hours. The depletion of Axl kinase by siRNA was confirmed by anti-Axl Western blot analysis. Independent of the conditions, an increase of pHER3 Y1289 levels was evident in contrast to control treatments. Tubulin served as loading control. (E) Met-specific knockdown displayed no effect on pHER3 Y1289 levels compared to control siRNA treatment. The phosphorylation of HER3 Y1289 was induced by 10 μM BMS777607 treatment for 24 hours independent of Met expression. The depletion of Met kinase from the cells was confirmed by Western blot analysis performed on cell lysates harvested 48 hours after Met-specific siRNA transfection. Tubulin served as loading control.

were determined from dose-response curve generated by four-parameter curve fitting. For statistical analysis, we performed a Mann-Whitney test or a Kruskal-Wallis test in combination with

Dunn multiple comparison posttest using GraphPad Prism 5 (GraphPad Software, Inc, La Jolla, CA). Differences with $*P < .05$, $**P < .01$, and $***P < .001$ were considered as statistically significant.

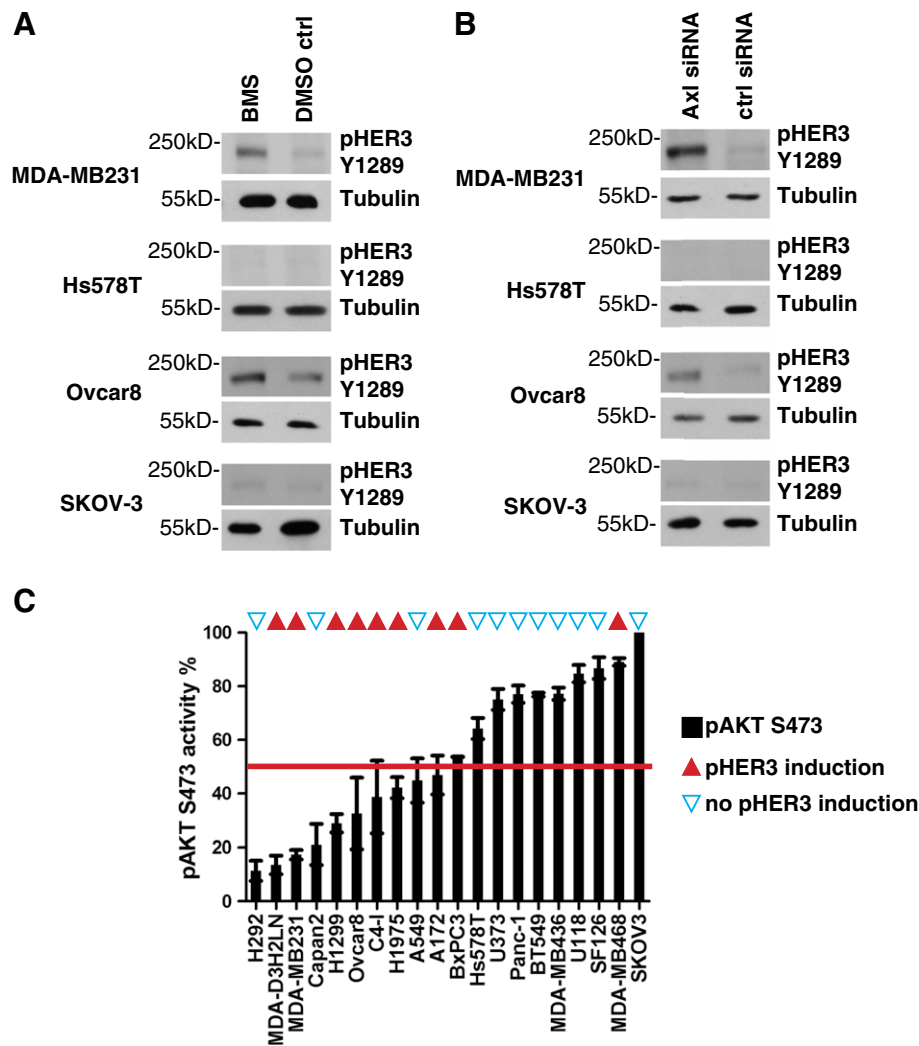


Figure 3. Inhibition of Axl leads to phosphorylation of HER3 in multiple cell lines and correlates with low basal AKT phosphorylation. (A) Western blot analysis of MDA-MB231, Hs578T, Ovarc8, and SKOV-3 cells treated with 10 μ M BMS777607 for 24 hours. A significant increase of pHER3 Y1289 levels was evident in MDA-MB231 and Ovarc8 cells in contrast to Hs578T and SKOV-3 cells. Tubulin served as loading control. (B) Western blot analysis of MDA-MB231, Hs578T, Ovarc8, and SKOV-3 cells treated with Axl-specific siRNA for 48 hours. A significant increase of pHER3 Y1289 levels was evident in MDA-MB231 and Ovarc8 cells in contrast to Hs578T and SKOV-3 cells. Tubulin served as loading control. (C) Low basal levels of AKT S473 phosphorylation correlate with induction of pHER3 Y1289 after Axl inhibition by 10 μ M BMS777607 and Axl knockdown with siRNA. The levels of basal AKT S473 phosphorylation for the indicated 20 cell lines are shown in ascending order on the abscissa axis. In parallel, we determined the up-regulation of HER3 phosphorylation of those 20 cell lines by Western blot analysis for pHER3 Y1289. The cell lines displaying activation of HER3 after Axl depletion were marked with red triangles on the top. The cell lines without HER3 response to Axl inactivation were marked with blue triangles. A positive correlation between a low basal phosphorylation of AKT S473 and the induction of HER3 phosphorylation was evident as 7 of 10 cell lines with low pAKT S473 levels, but only 2 of 10 cell lines with high pAKT S473 levels responded with up-regulation of pHER3 Y1289 to the inhibition of Axl by BMS777607 or Axl-specific siRNA. AKT phosphorylation was normalized to the highest values represented by SKOV3 cells (100%). Mean values and SEM are shown ($n = 3$).

Results

Inhibition of the Axl RTK Leads to Up-Regulation of HER3 Phosphorylation

The Axl RTK activates prosurvival and metastatic pathways, and Axl overexpression was shown to correlate with aggressive tumor behavior. Therefore, we evaluated multiple TKI as potential Axl inhibitors and finally selected BMS777607 as the most potent Axl inhibitor published up to now. BMS777607 is currently undergoing phase I clinical trials and was originally described as a Met TKI. However, BMS777607 displays a higher affinity to Axl RTK (IC_{50} of

1.1 nM) than to Met (IC_{50} of 3.9 nM) as published by Schreoder et al., 2009 [24]. In the first step, we validated the efficiency of BMS777607 to inhibit Axl phosphorylation by treating Axl-overexpressing NIH/3T3-Axl cells for 1 hour with serially diluted compound concentrations. Subsequently, we performed a phospho-Axl-specific ELISA and calculated the IC_{50} values by applying a four-parameter logistic curve fit. BMS777607 inhibits Axl autophosphorylation at low nanomolar concentrations, displaying an IC_{50} value of 0.006 μ M as shown in Figure 2A. This NIH/3T3-Axl cell line was generated by Axl cDNA transfection because it represents a useful tool to screen the efficacy of Axl inhibitors.

For the subsequent experiments, we used MDA-MB231 cells as a model system to study the effect of Axl inhibitors on human cancer cells. We selected the triple-negative breast cancer cell line MDA-MB231, first, because it is characterized by overexpression of the Axl RTK, and second, because multiple studies proved in MDA-MB231

cells that aggressive cell behavior depends on the expression of Axl RTK [14,26,27]. To confirm the activity of BMS777607 on MDA-MB231 cells and to analyze the activation pattern of other RTKs after Axl inhibition, we performed Human Phospho-RTK arrays. Therefore, we depleted Axl protein by Axl-specific siRNA knockdown or blocked Axl

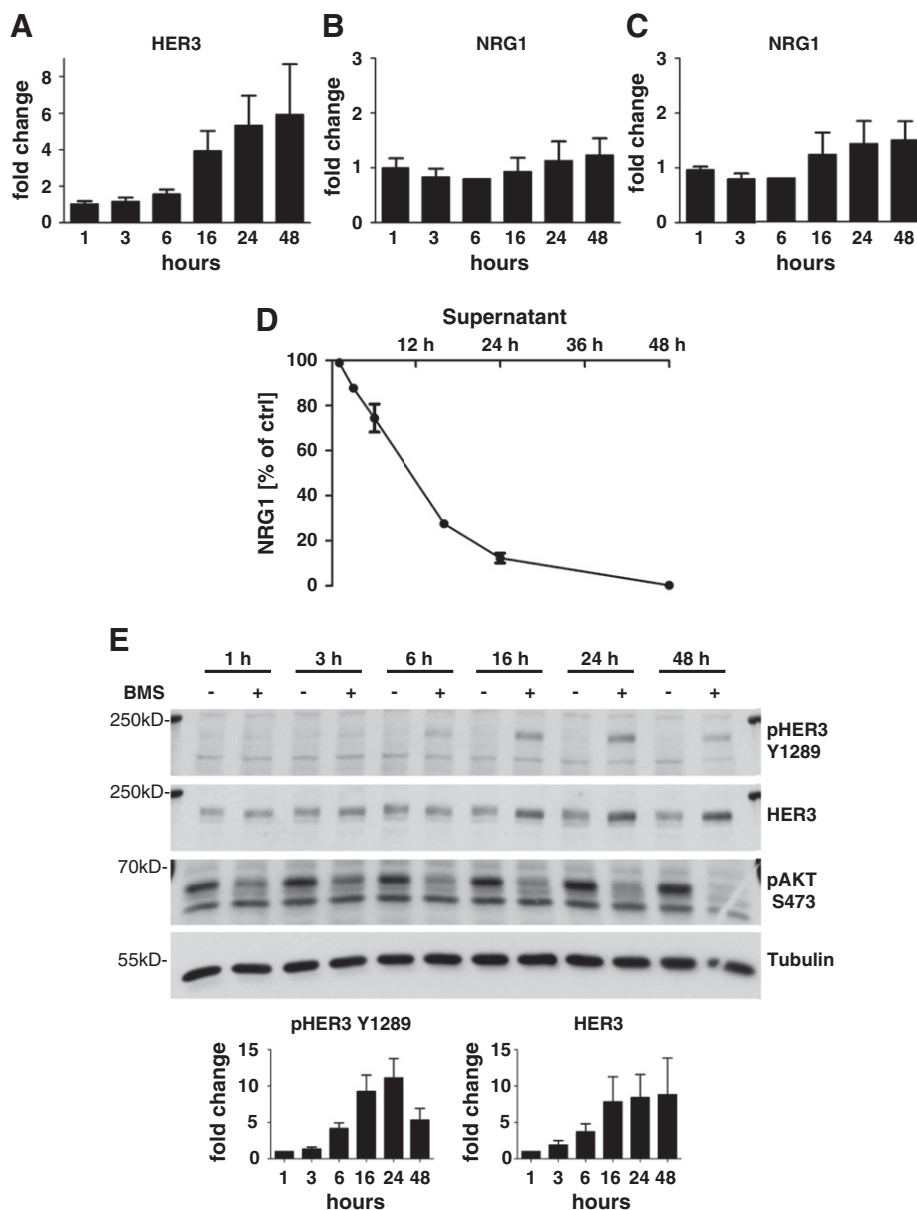


Figure 4. Inhibition of the Axl RTK activates HER3 transcription and phosphorylation. HER3 correlates with consumption of NRG1. (A) Quantification of HER3 mRNA induction in MDA-MB231 cells. Cells were treated with 10 μ M BMS777607 for 1 hour up to 48 hours. A three- to six-fold increase of HER3 mRNA was evident between 16 to 48 hours posttreatment. Mean values and SEM are shown ($n = 3$). (B) Quantification of NRG1 mRNA induction with primer set 1 detecting all isoforms of NRG1 except isoforms No. 2 and No. 14. Cells were treated with 10 μ M BMS777607 for 1 hour up to 48 hours. No significant increase of NRG1 mRNA levels was detected. Mean values and SEM are shown ($n = 3$). (C) Quantification of NRG1 mRNA induction with primer set 2 detecting isoforms No. 2, No. 15, and No. 17 of NRG1. Cells were treated with 10 μ M BMS777607 for 1 hour up to 48 hours. No significant increase of NRG1 mRNA levels was detected. Mean values and SEM are shown ($n = 3$). (D) Quantification of NRG1 protein levels in conditioned medium was assayed using NRG1-ELISA. Cells were treated with 10 μ M BMS777607 for 1 to 48 hours. A time-dependent consumption of NRG1 was measured. Mean values and SEM are shown ($n = 3$). (E) Western blot analysis of MDA-MB231 cells. Cells were treated with 10 μ M BMS777607 for 1 to 48 hours. A significant increase of the pHER3 Y1289 levels was evident in MDA-MB231 after 6 hours of treatment. The up-regulation of HER3 protein expression was evident 16 hours posttreatment. BMS777607 treatment continuously suppressed the phosphorylation of AKT S473. Tubulin served as loading control. The diagrams show the densitometric analysis of Western blots for pHER3 Y1289 and HER3. Mean values and SEM are shown ($n = 3$).

tyrosine kinase activity by BMS777607 treatment. Surprisingly, 24 hours after exposure of MDA-MB231 cells to 1 μ M BMS777607, phosphorylation of Axl and Met decreased significantly, whereas phosphorylation of HER3 was markedly enhanced. The phosphorylation of the other three HER family members (EGFR, HER2, and HER4) remained unchanged (Figure 2B). In contrast to the treatment with 1 μ M BMS777607, the Axl-specific siRNA knockdown additionally induced the phosphorylation of the insulin receptor (InR) and a slight up-regulation of the insulin-like growth factor 1 receptor (IGF1R) and of HER2 levels (Figure 2B). Unfortunately, we were not able to verify the phosphorylation of InR, IGF1R, and HER2 in Western blot experiments (data not shown).

To validate this Axl-specific siRNA-induced HER3 phosphorylation, we performed an immunoprecipitation for HER3 from MDA-MB231 cell lysates under the same conditions as described for the RTK array. Tyrosine phosphorylation of HER3 was quantified by Western blot analysis using a homemade anti-p-Tyr antibody. The same induction of HER3 phosphorylation was evident with the site-specific pHER3 Y1289 antibody (Figure 2C). pHER3 Y1289 is a PI3K-binding site, and this phosphorylation was shown to be essential for PI3K/AKT signaling cascade activation [28]. Therefore, we used this site-specific antibody for all subsequent experiments.

To further validate the RTK array results and to elucidate the impact of serum on HER3 phosphorylation, we treated MDA-MB231 cells with Axl-specific siRNA to induce depletion of Axl protein either under full-serum conditions (10% FBS) or under starving conditions (0% FBS). The depletion of Axl kinase from the cells was confirmed by Western blot analysis performed on cell lysates harvested 48 hours after Axl-specific siRNA transfection. Independent of the serum conditions, a significant increase of pHER3 Y1289 levels was evident in contrast to control siRNA treatment (Figure 2D). The treatment with 1 and 10 μ M BMS777607 for 24 hours led also to an enhancement of HER3 phosphorylation in a concentration-dependent manner (Figure 2D).

As BMS777607 was originally published as Met inhibitor but also targets Axl RTK very potently at low nanomolar concentrations, it was necessary to elucidate a possible role of Met in the up-regulation process of phospho-HER3 [24]. Therefore, we used Met-specific siRNA to deplete the protein from MDA-MB231 cells. The Met knockdown was confirmed by Western blot analysis 48 hours after Met-specific siRNA transfection. Met knockdown displayed no effect on pHER3 Y1289 levels compared to control siRNA treatment (Figure 2E). Additionally, independent from the Met knockdown, the treatment with 10 μ M BMS777607 for 24 hours increased the phosphorylation level of HER3. On the basis of this result, we conclude that Met inhibition is not related to the up-regulation of HER3 phosphorylation.

To sum up, HER3 remained the only validated and consistently up-regulated RTK after treatment with BMS777607 or knockdown with Axl-specific siRNA in MDA-MB231 cells.

Inhibition of Axl RTK Leads to Phosphorylation of HER3 in Multiple Cell Lines and Correlates With Low Basal AKT Phosphorylation

Because we had shown that pHER3 is an activating feedback mechanism on Axl inhibition in MDA-MB231 cells, we asked if this is a general phenomenon in Axl-overexpressing tumor cells. Therefore, we analyzed the activation of HER3 in different breast and ovary cancer cell lines expressing Axl. First, we blocked Axl activity pharmacologically

with 10 μ M BMS777607 (Figure 3A), and second, we depleted Axl protein by Axl-specific siRNA (Figure 3B). Phospho-HER3 was inducible after Axl protein depletion as well as after inhibition of phosphorylation by treatment with 10 μ M BMS777607 in MDA-MB231 and Ovarc8 cells but not in Hs578T and SKOV-3 cells (Figure 3, A and B). From this finding, we concluded that Axl expression itself is not a biomarker for the induction of a HER3 feedback loop.

To further characterize the HER3 activation loop, we analyzed 20 different Axl-expressing cell lines originating from brain, breast, ovary, cervix, lung, and pancreatic tumors. Knowing that the AKT signaling pathway is influenced by Axl RTK, we performed phospho-AKT S473 ELISAs to determine the basal AKT phosphorylation levels. The levels of pAKT S473 are shown in ascending order on the axis of abscissas in Figure 3C. In parallel, we determined the activation of HER3 in those 20 cell lines after treatment with 10 μ M BMS777607 and Axl-specific siRNA by Western blot analysis with the pHER3 Y1289 antibody. The cell lines displaying activation of HER3 after Axl depletion were marked with red triangles on the top of Figure 3C. The cell lines without HER3 response to Axl inactivation were marked with blue triangles. Thereby, we discovered a positive correlation between a low basal phosphorylation of AKT S473 and the induction of HER3 activation on Axl inhibition by BMS777607 and Axl-specific siRNA treatment. Seven of 10 cell lines with low pAKT S473 levels but only 2 of 10 cell lines with high pAKT S473 levels responded with up-regulation of pHER3 Y1289 after inhibition of Axl by BMS777607 or Axl-specific siRNA treatment (Figure 3C).

From these results, we conclude that inhibition of Axl induces an activation feedback loop of HER3, in various tumor types, characterized by low basal AKT S473 phosphorylation and by a high dependency on Axl/PI3K/AKT signaling.

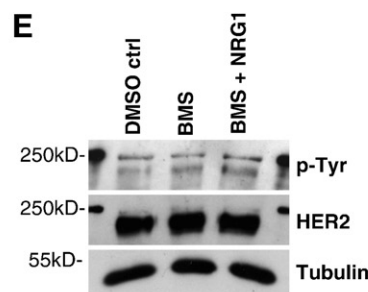
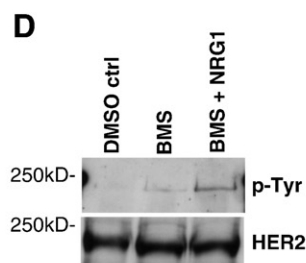
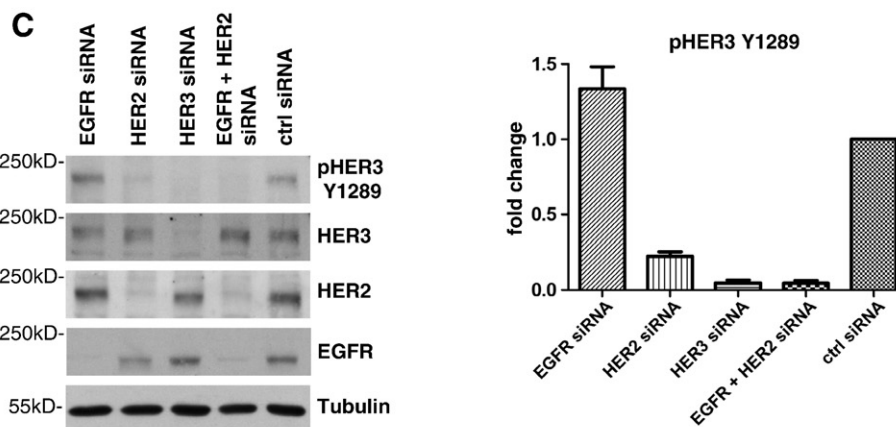
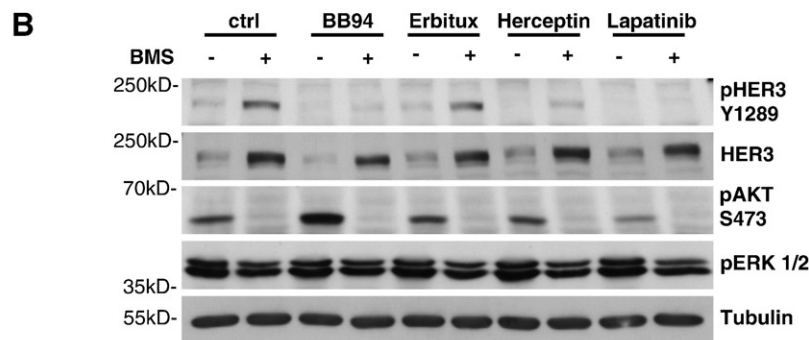
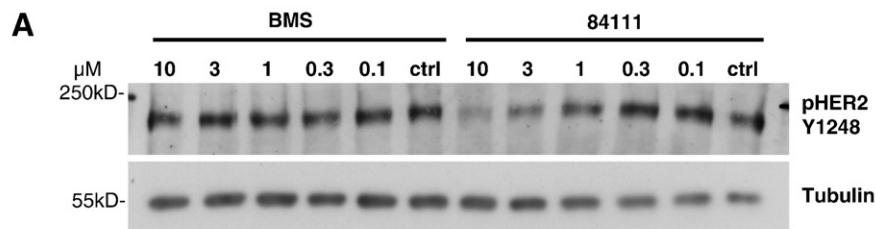
Inhibition of the Axl RTK Activates HER3 Transcription but Not of Its Ligand NRG1

Next, we performed quantitative PCR to determine the levels of HER3 mRNA. Therefore, we treated MDA-MB231 cells with 10 μ M BMS777607 and harvested them at different time points. A significant induction of HER3 mRNA production became evident after 16 hours of treatment reaching a 3.9-fold level, whereas the maximum increase of HER3 mRNA was achieved after 48 hours reaching 5.9-fold values (Figure 4A). As breast cancer cells often express high levels of HER RTK activating ligands [29], we performed quantitative PCR and ELISA analysis of the HER3 ligand NRG1 to compare the relative levels after treatment with 10 μ M BMS777607. The Gene database search on National Center for Biotechnology Information platform revealed 17 different NRG1 isoforms in *H. sapiens* (Gene ID: 3084). Due to the fact that NRG1 appears in different isoforms deriving from the *NRG1* gene by alternative splicing, we used two different primer sets for quantitative PCR analysis. One primer set binds to the mRNA of all isoforms except of isoforms No. 2 and No. 14. The second primer set binds to the mRNA of isoforms No. 2, No. 15, and No. 17. In this way, we were able to cover all isoforms with the exception of isoform No. 14. NRG1 mRNA expression was detectable in MDA-MB231 cells, but it was induced only reaching values between 1.2- or 1.5-fold within 48 hours (Figure 4, B and C). Accordingly, we excluded NRG1 mRNA up-regulation as being responsible for HER3 activation.

Induction of HER3 Phosphorylation Correlates with Consumption of NRG1

Although we did not expect an up-regulation of NRG1 ligand on the basis of the quantitative PCR results, we analyzed NRG1 protein levels in the supernatant of BMS777607-treated MDA-MB231 cells by NRG1-ELISA. Strikingly, the levels of NRG1 protein dropped in the supernatant of 10 μ M BMS777607-treated MDA-MB231 cells in a time-dependent manner compared to DMSO-treated control levels from 97% after 1 hour to less than 1% after 48 hours (Figure 4D). To determine if there is any connection between the decrease of NRG1 ligand in the supernatant and HER3 activation, we treated the MDA-MB231 cells in a time course experiment up to 48 hours with 10 μ M BMS777607 and analyzed in parallel the supernatant by Western blot. Consistent with the previous results,

BMS777607 caused a 4.2-fold activation of pHER3 Y1289 after 6 hours of treatment (Figure 4E). The activation of pHER3 Y1289 correlated with the decrease of NRG1 in the supernatant (Figure 4D). The climax of 11.1-fold HER3 activation was reached after 24 hours of compound treatment and decreased at the 48-hour time point. Parallel to the pHER3 Y1289 decrease, NRG1 levels of the supernatant approximated the background level of the NRG1 ELISA assay after 48 hours. At the same time, we proved that the 7.8- to 8.8-fold increased expression of HER3 protein, after 16 to 48 hours of treatment, results from the elevated level of HER3 mRNA as shown in Figure 4A. Simultaneously, BMS777607 was able to inhibit phosphorylation of AKT S473 constantly for up to 48 hours. However, the phosphorylation of HER3 does not result in a downstream activation of pAKT S473. These results reveal that Axl



inhibition by BMS777607 leads to transcription of HER3 protein and to the NRG1 ligand-dependent phosphorylation of HER3. Additionally, these results are in line with the mechanism of AKT inhibition-dependent transcription of HER3 described recently by Chandralapty et al., 2011 and Chakrabarty et al., 2012 [30,31].

HER3 Induction is a Common Feedback Mechanism of Axl Inhibitors

Because we could show that induction of pHER3 is part of an activation feedback mechanism induced by BMS777607, we asked whether this is a general phenomenon of Axl inhibitors. Therefore, we compared BMS777607 to R428, a recently described Axl inhibitor [25], and an Axl inhibitor recently developed by our group, namely, MPCD84111. First, we determined the activity of these Axl TKIs in NIH/3T3 Axl-overexpressing cells. For this reason, we treated the cells for 1 hour with serially diluted compound concentrations of BMS777607, MPCD84111, and R428 and subsequently performed a phospho-Axl-specific ELISA to calculate the IC₅₀ values by applying a four-parameter logistic curve fit. As shown in Figure 1A, the compounds inhibited Axl phosphorylation at nanomolar concentrations, displaying IC₅₀ values for BMS777607 of 0.006 μM, MPCD84111 of 0.027 μM, and R428 of 0.043 μM.

Next, we analyzed if MPCD84111 and R428 have the same impact on the HER3 feedback loop as BMS777607 in MDA-MB231 cells. Interestingly, treatment with 10 μM BMS777607 and 10 μM R428 induced the phosphorylation of HER3 (6.7- and 2.8-fold), whereas 10 μM MPCD84111 prohibited the phosphorylation of HER3 by 68% in comparison to DMSO control within 24 hours (Figure 1B). We could also demonstrate that 10 μM BMS777607 and 10 μM R428 as well as 10 μM MPCD84111 induce HER3 expression 6.1-, 7.5-, and 7.4-fold in comparison to DMSO treatment. Our data reveal that the transcriptional feedback loop of HER3 was initiated similarly by BMS777607, R428, and MPCD84111, even though MPCD84111 was able to block phosphorylation of HER3 Y1289 efficiently.

To elucidate these results in more detail, we treated MDA-MB231 cells in a time course experiment for up to 48 hours with 1 μM BMS777607 or MPCD84111 and analyzed the cell lysates by Western blot. In contrast to BMS777607, MPCD84111 inhibited the phosphorylation of HER3 Y1289 during the entire time course (Figure 1C). Interestingly, both inhibitors increased the total protein levels of HER3 after 16 hours of treatment. It was published earlier by Myatt and Lam, 2007 that inhibition of AKT has an impact on the expression and activity of the Forkhead box protein O (FoxO) family members [32]. Therefore, the induction of HER3 RTK expression might result from FoxO-dependent transcription. Our data point out that the phosphorylation of HER3 is blocked by MPCD84111 independently from transcription cascade of HER3 and might result from a direct inhibition by the compound.

MPCD84111 Inhibits the Dimerization Partner for HER3

Subsequently, we addressed the question why MPCD84111, but not BMS777607, inhibits phosphorylation of HER3. It is widely accepted that HER3 has an impaired kinase activity. Because of this reason, activation of the HER3 RTK occurs only after the dimerization with other RTKs, such as HER2 or EGFR [33]. We asked if MPCD84111-dependent inhibition of HER3 phosphorylation (Figure 1, B and C) might be a result of blocking HER2 as a heterodimerization partner for HER3. Therefore, we determined the kinase selectivity profile of MPCD84111 using three different types of assays, namely, IMAP, binding, and HTRF assays. The kinase profile of BMS777607 was published earlier by Schroeder et al., 2009 [24]. The kinase profile of MPCD84111 displayed an inhibition of Axl as well as Met, Src, Abl, Kit, Ret, PDGFRβ, Tie2, VEGFR-2, and DDR1 with efficacy of 100% when used at 10 μM concentration (Figure 1D). The comparison of both kinase selectivity profiles identified common targets of BMS777607 and MPCD84111 such as Axl, Met, Kit, PDGFRβ, Tie2, AuroraA/B, and VEGFR-2. In contrast to BMS777607, MPCD84111 uniquely targets HER2, a

Figure 5. Inhibition of HER2 blocks HER3 phosphorylation in triple-negative breast cancer cells. (A) Validation of HER2 being a target of MPCD84111. MPCD84111 inhibits phosphorylation of HER2 in contrast to BMS777607 as demonstrated on HER2-expressing MCF7 cells. Phosphorylation of HER2 Y1248 was analyzed 1 hour after addition of BMS777607 and MPCD84111 by Western blot. Both compounds were used in three-fold serial dilutions starting with 10 μM. Tubulin served as loading control. (B) Herceptin and lapatinib block HER3 phosphorylation in MDA-MB231 cells. Representative Western blots of MDA-MB231 cells treated with 10 μM BMS777607 for 24 hours compared to DMSO-treated control cells are shown. Cells were additionally incubated with 5 μM BB94 (batimastat), 10 μg/ml Erbitux, 10 μg/ml Herceptin, or 5 μM lapatinib for 2 hours. One hundred micrograms of lysate was subjected to sodium dodecyl sulfate-polyacrylamide gel electrophoresis, blotted, and probed with corresponding antibodies for pHER3 Y1289, HER3, pAKT S473, pERK1/2, and Tubulin as loading control. BB94, Herceptin, and lapatinib were able to suppress the BMS777607-induced HER3 Y1289 phosphorylation in contrast to Erbitux. (C) EGFR in combination with HER2-specific knockdown exhibits a significant effect on pHER3 Y1289 levels compared to control siRNA treatment. MDA-MB231 cells were treated with EGFR, HER2, HER3, and a combination for EGFR and HER2-specific siRNA for 48 hours. Subsequently, the phosphorylation of HER3 Y1289 was induced by 10 μM BMS777607 treatment for 24 hours. Only HER3 and the combination of EGFR and HER2 siRNA blocked HER3 phosphorylation completely. HER2-specific knockdown leads to a less pronounced reduction of HER3 phosphorylation, and EGFR-specific knockdown even induces pHER3 Y1289 activity by 1.4-fold. The depletion of EGFR, HER2, and HER3 from the cells was confirmed by Western blot analysis. Tubulin served as loading control. The diagram shows the densitometric analysis of Western blots for pHER3 Y1289. Mean values and SEM are shown ($n = 3$). (D) MDA-MB231 cells were treated with 10 μM BMS777607 for 24 hours to further validate the involvement of HER2 in the phosphorylation of HER3. The HER2 RTK was immunoprecipitated with a commercial HER2-specific antibody (Millipore, No. 06-562) from 2 mg of total lysate. Western blots for p-Tyr and total HER2 are shown. BMS777607 treatment increased the phosphorylation of HER2 compared to DMSO-treated control, and 50 ng/ml NRG1 further enhanced the phosphorylation level. (E) Validation of HER2 activity by immunoprecipitation of HER2. MDA-MB231 cells were treated with 10 μM BMS777607 for 24 hours. The HER2 RTK was immunoprecipitated with a homemade HER2-specific antibody (clone 13D1B1) from 2 mg of total lysate. Western blots for p-Tyr, HER2, as well as for Tubulin are shown. Twenty micrograms of the total lysate was used for the Tubulin Western blot analysis as loading control for the immunoprecipitation. BMS777607 treatment increased the phosphorylation of HER2 compared to DMSO-treated control, and 50 ng/ml NRG1 further enhanced the phosphorylation level. Therefore, HER2 remains a hardly detectable, but active dimerization partner for HER3 in MDA-MB231 cells.

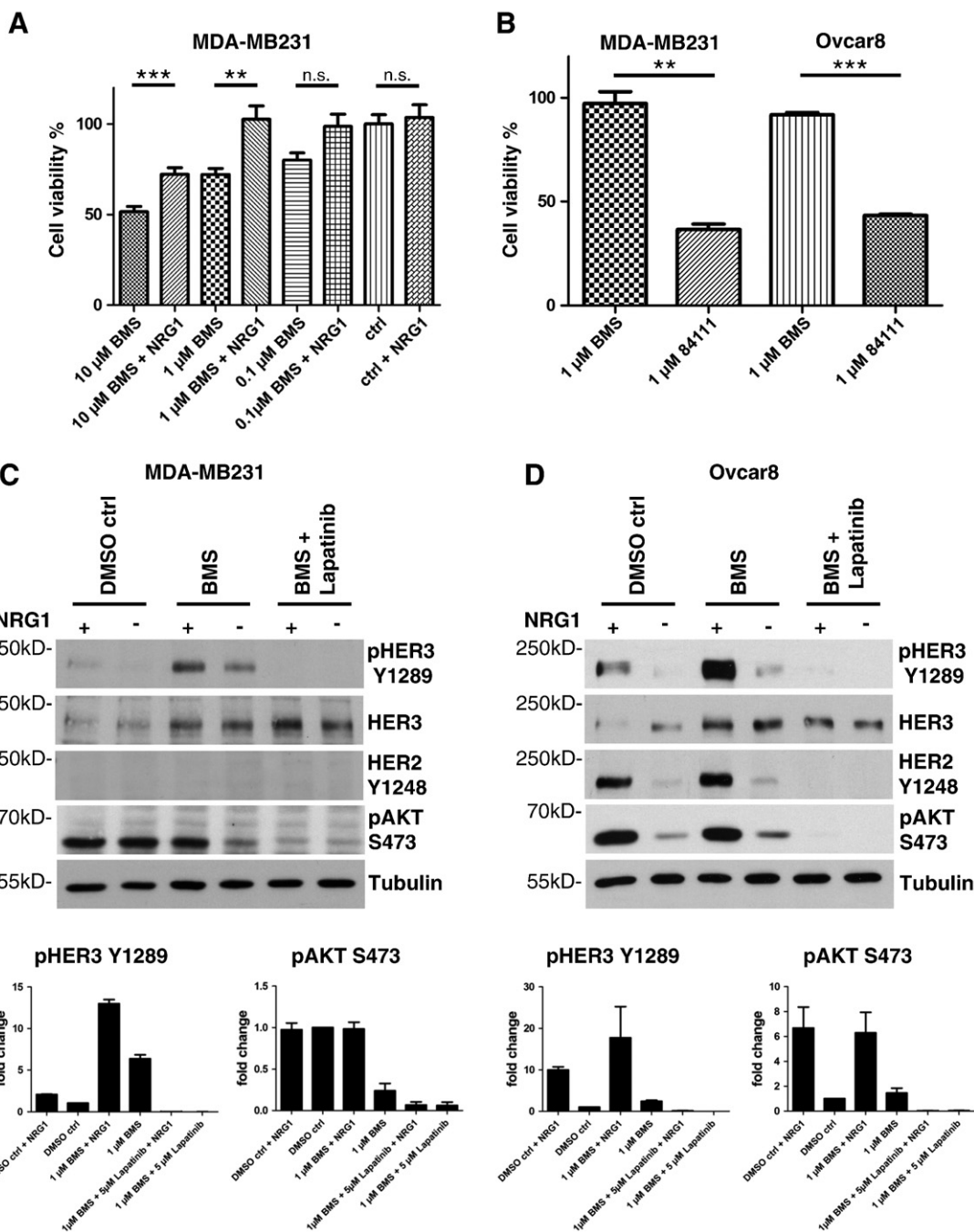
dimerization partner of HER3 (Figure 1D). This finding implicates that blocking of HER3 phosphorylation by MPCD84111 might be achieved by inhibition of HER2.

Inhibition of HER2 Blocks HER3 Phosphorylation in Triple-Negative Breast Cancer Cells

In breast cancer cells with HER2 gene amplification, HER2 is the main kinase that phosphorylates HER3 [34]. As BMS777607 in contrast to MPCD84111 does not affect the catalytic activity of HER2 as demonstrated in MCF7 cells expressing HER2 (Figure 5A), we assumed that in HER2 low-expressing MDA-MB231 cells, HER2 might also act as the kinase maintaining phosphorylation of HER3 on inhibition of Axl as well.

Therefore, we examined the effect of BMS777607 in combination with either 10 µg/ml HER2-blocking antibody Herceptin, 5 µM

EGFR/HER2 TKI lapatinib, or 5 µM the broad spectrum matrix metalloprotease inhibitor BB94 (batimastat). In MDA-MB231 cells, all of these combinations effectively inhibited phosphorylation of HER3, in contrast to the treatment with 10 µg/ml Erbitux (Figure 5B). Particularly, the specific blocking of HER2 by the monoclonal antibody Herceptin as well as lapatinib suggested that HER2 plays a significant role in maintaining phosphorylation of HER3 in MDA-MB231 cells. It is well known that active ligands of the HER family are proteolytically cleaved by metalloproteases and afterwards released from the cell surface [35]. BB94 (batimastat) is a broadband inhibitor of the Disintegrin and metalloproteinase domain-containing protein ADAM family of metalloproteases and blocks shedding of EGFR ligands [36,37]. Inhibition of HER3 phosphorylation by 5 µM BB94 underlined our findings that HER3 is activated by an extracellular mechanism. BMS777607 consistently



blocked phosphorylation of AKT S473 but had only a minor effect on the Mitogen-activated protein-kinase pathways as proven by pERK1/2 Western blot analysis (Figure 5B).

Knowing that lapatinib was most efficient in blocking HER3 phosphorylation, we evaluated the impact of EGFR and HER2 on HER3 phosphorylation by siRNA experiments. Therefore, we depleted EGFR, HER2, HER3, and EGFR in combination with HER2 from MDA-MB231 cells by siRNA knockdown and subsequently induced HER3 phosphorylation by 10 μ M BMS treatment for 24 hours (Figure 5C). Only HER3 siRNA and the combination of EGFR and HER2 siRNA treatment blocked HER3 phosphorylation, completely exhibiting less than 5% of phosphorylation compared with control siRNA treatment. Comparable to Herceptin, HER2-specific siRNA treatment remained a residual HER3 phosphorylation of 22% (Figure 5C).

Although MDA-MB231 cells represent a prototype of triple-negative breast cancer cell lines characterized by the loss of HER2 expression, we investigated HER2 as one of the probable dimerization partners of HER3. To elucidate in more detail the phosphorylation status of HER2 in triple-negative breast cancer cells, we performed immunoprecipitation experiments with a vast protein amount of 2 mg. We treated MDA-MB231 cells with 10 μ M BMS777607 for 24 hours, and we further enhanced the phosphorylation of HER2 by stimulation with 50 ng/ml NRG1. The HER2 RTK was immunoprecipitated with a homemade anti-HER2-specific antibody (clone 13D1B1) or a commercial anti-HER2 antibody (Millipore, No. 06-562). The subsequent Western blot analysis for p-Tyr resulted in a slight, but reproducible, induction of tyrosine phosphorylation after BMS777607 treatment and NRG1 stimulation (Figure 5, D and E).

Hence, we assume that this minimal amount of HER2 phosphorylation might contribute to the pronounced HER3 activation and thereby maintains the feedback loop counteracting Axl inhibitor treatment. Additionally, lapatinib emerged as the most efficient treatment strategy for inhibition of HER3 phosphorylation.

Exogenous Application of NRG1 Rescues AKT Phosphorylation and Cell Viability

Even though complete recovery of pAKT S473 was not achieved with a pharmacological dose of 1 μ M BMS777607, the feedback up-regulation of HER3 expression and HER3 phosphorylation was clearly evident, further suggesting that inhibition of the Axl/PI3K/AKT pathway leads to the reactivation of HER3 (Figure 4E). These data imply that HER3 phosphorylation partially restores the pro-survival and proliferation signaling that, in turn, may limit the effect of Axl inhibitors. To support this hypothesis, we performed rescue experiments in combination with cell viability assays. MDA-MB231 cells were treated with pharmacological concentrations of BMS777607 under starving conditions for 72 hours. Addition of the HER3 ligand (50 ng/ml NRG1) completely compensated the inhibitory effect of 0.1 and 1 μ M BMS777607 on cell viability. In contrast, the cell viability of the untreated cells was not affected by NRG1 stimulation (Figure 6A). The compensatory up-regulation of HER3 expression and partial maintenance of HER3 phosphorylation on inhibition of Axl suggested that combined inhibition of Axl and HER2/HER3 could synergistically inhibit tumor cell viability.

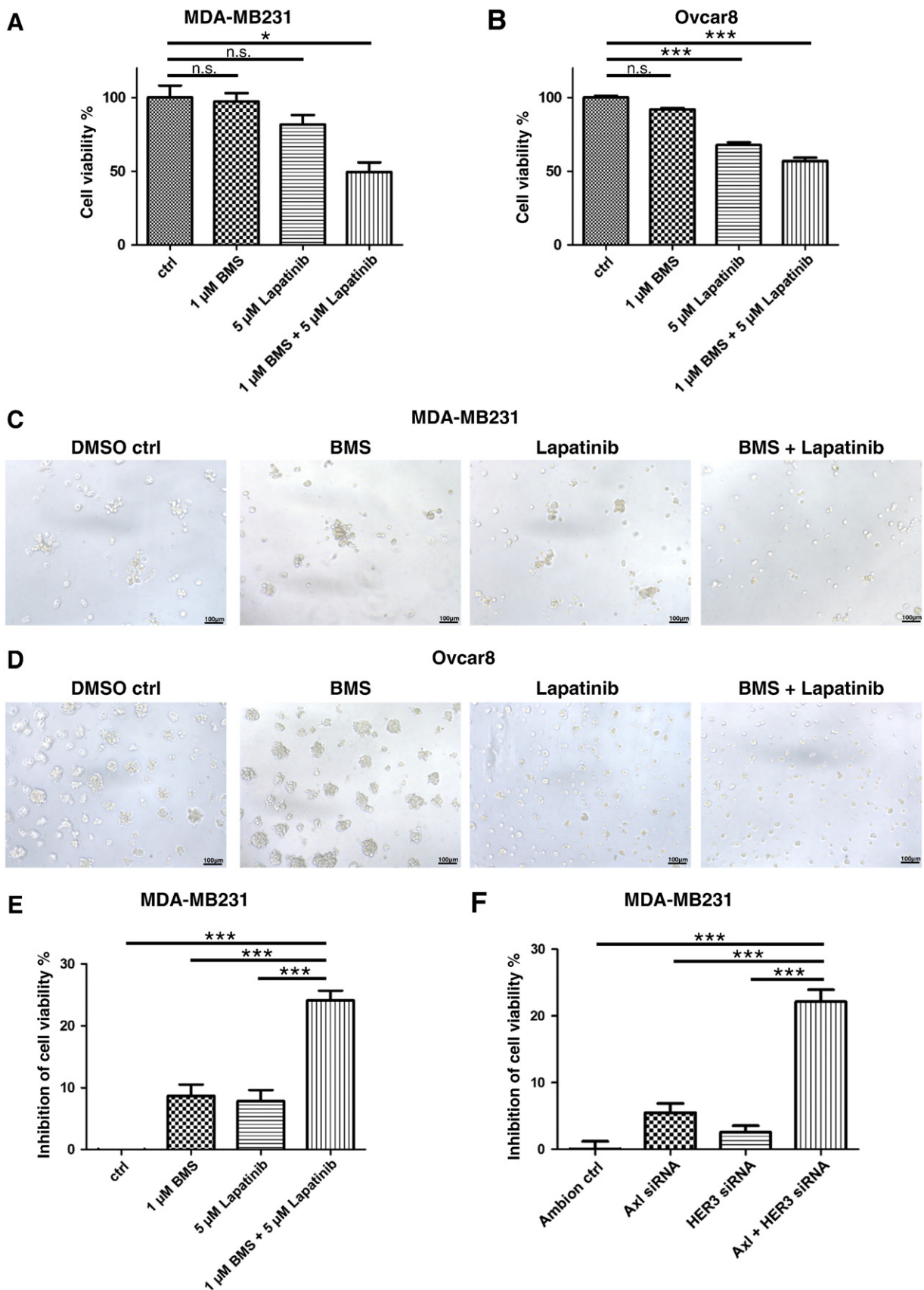
Monolayer cell cultures represent oversimplified models for tumor studies, due to the loss of extracellular matrix rigidity on artificial plastic surfaces and high serum concentrations. These conditions poorly mimic the tumor cell biology *in vivo*. A more robust and reproducible test system is the three dimensional (3D) spheroid culture. To test the combined inhibition of Axl and HER2/HER3 on tumor cell viability, we used these 3D spheroid cultures.

We treated two Axl-expressing cell lines, namely MDA-MB231 and Ovar8, with MPCD84111 and with a combination of BMS and lapatinib, to elucidate the hypothesis that an inhibition of Axl and HER2/HER3 might be essential for treatment of Axl overexpressing cells. First, we proved the efficacy of 1 μ M MPCD84111 in contrast to 1 μ M BMS777607 treatment on MDA-MB231 and Ovar8 cells. One micromolar MPCD84111 significantly inhibited cell viability to 37% in MDA-MB231 spheroids and to 42% in Ovar8 spheroids in

Figure 6. Exogenous application of NRG1 rescues AKT phosphorylation and cell viability. (A) Exogenous application of NRG1 rescues the inhibition of cell viability by BMS777607. Cell viability of MDA-MB231 cells was measured by CellTiter-Glo assay after 72 hours of treatment under starving conditions (0% FBS). Cells were incubated with increasing concentrations of BMS777607 (0.1, 1, 10 μ M) with and without 50 ng/ml NRG1. Addition of NRG1 completely compensates the proliferation inhibitory function of 0.1 and 1 μ M BMS777607. The DMSO control does not react to NRG1 stimulation. Mean values and SEM of three independent experiments are shown. Differences with * P < .05, ** P < .01, and *** P < .001 were considered statistically significant (Mann-Whitney test; ns, nonsignificant). (B) Cell viability of MDA-MB231 and Ovar8 cells is inhibited by MPCD84111 in contrast to BMS777607. Cell viability of MDA-MB231 and Ovar8 cells was measured by CellTiter-Glo assay after 72 hours of treatment. 3D spheroids were incubated with 1 μ M BMS777607 or 1 μ M MPCD84111 using starving conditions (0% FBS). Cell viability was reduced to 37% by MPCD84111 in MDA-MB231 cells and to 43% in Ovar8 cells. Mean values and SEM of three independent experiments are shown. Differences with * P < .05, ** P < .01, and *** P < .001 were considered statistically significant (Mann-Whitney test). (C) BMS777607 and lapatinib exhibit a synergistic inhibitory effect on HER3 phosphorylation. Western blot analysis of MDA-MB231 cells is shown. Cells were treated with 1 μ M BMS777607 or a combination of 1 μ M BMS777607 and 5 μ M lapatinib relative to DMSO control for 24 hours with or without 50 ng/ml NRG1 stimulation for 15 minutes. A significant increase of the pHER3 Y1289 levels was evident after BMS777607 treatment. BMS777607 treatment suppressed the phosphorylation of AKT S473 to 24%. Additional NRG1 stimulation enhances HER3 phosphorylation and restores pAKTS473 phosphorylation. The combination of BMS777607 and lapatinib blocks completely the HER3 and AKT phosphorylation. Tubulin served as loading control. The diagrams show the densitometric analysis of Western blots for pHER3 Y1289 and pAKT S473. Mean values and SEM are shown (n = 3). (D) BMS777607 and lapatinib exhibit a synergistic inhibitory effect on HER3 phosphorylation. Western blot analysis of Ovar8 cells is shown. Cells were treated with 1 μ M BMS777607 or a combination of 1 μ M BMS777607 and 5 μ M lapatinib relative to DMSO control for 24 hours with or without 50 ng/ml NRG1 stimulation for 15 minutes. A 2.4-fold increase of the pHER3 Y1289 levels was evident after BMS777607 treatment. BMS777607-induced HER phosphorylation treatment completely rescued AKT phosphorylation. Additional NRG1 stimulation enhances HER3 and pAKTS473 phosphorylation. The combination of BMS777607 and lapatinib blocks completely the HER3 and AKT phosphorylation. Tubulin served as loading control. The diagrams show the densitometric analysis of Western blots for pHER3 Y1289 and pAKT S473. Mean values and SEM are shown (n = 3).

contrast to 1 μ M BMS777607 treatment exhibiting cell viability rates of 97% in MDA-MB231 and 92% in Ovc8r in comparison to DMSO-treated controls (Figure 6B).

Second, we proved the complete inhibition of HER3 phosphorylation by combined treatment of 1 μ M BMS777607 and 5 μ M lapatinib in MDA-MB231 and Ovc8r cells. Additionally, we analyzed



if BMS treatment or the stimulation with HER3 ligand NRG1 might lead to the reconstitution of the AKT signaling pathway.

One micromolar BMS777607 leads to up-regulation of total HER3 protein levels and to a six-fold induction of HER3 phosphorylation after 24 hours of treatment in MDA-MB231 cells (Figure 6C). The phospho-AKTS473 levels are reduced to 24% compared with DMSO-treated cells, and additional stimulation with 50 ng/ml NRG1 restores pAKTS473 signal to DMSO control levels. The combination of 1 μ M BMS777607 and 5 μ M lapatinib inhibited HER3 and AKT phosphorylation to 0.9%, respectively, 6.1% in comparison to BMS777607 single treatment. Especially, NRG1 ligand stimulation was not able to induce HER3 phosphorylation any more than in contrast to DMSO (two-fold induction) and 1 μ M BMS777607 treatment (13-fold induction). HER2 phosphorylation was below detection threshold in MDA-MB231 cells due to the low expression level of HER2 in this cell line (Figure 6C).

The Ovarc8 cells react to 1 μ M BMS777607 treatment, analogous to MDA-MB231, by up-regulation of total HER3 protein levels and a 2.4-fold HER3 phosphorylation compared to DMSO-treated cells. This HER3 phosphorylation results in a 1.4-fold induction of AKT phosphorylation. Additional 50 ng/ml NRG1 ligand stimulation leads in a 10- or 17.8-fold HER3 phosphorylation in DMSO control and 1 μ M BMS777607-treated cells. The combined treatment with 1 μ M BMS777607 and 5 μ M lapatinib completely prevents HER3 and AKT phosphorylation and additionally prohibits the activation by NRG1 ligand. In Ovarc8 cells, HER2 Y1248 exhibits an identical phosphorylation pattern to pHER3 Y1289, emphasizing the importance of the HER2/HER3 heterodimer in maintaining the Her3 phosphorylation in cell lines with significant HER2 levels (Figure 6D).

We conclude that BMS777607-induced HER3 phosphorylation is able to rescue or at least stabilizes the AKT signaling in Ovarc8 and MDA-MB231 cells, and *vice versa*, a combination of 1 μ M BMS777607 and 5 μ M lapatinib completely inhibits HER3 and AKT phosphorylation.

Pharmacological Inhibition of Axl Sensitizes for Lapatinib Treatment

We further tested the combined inhibition of Axl and HER2/HER3 on tumor cell viability in 3D spheroid cultures of MDA-MB231 and Ovarc8 cells. Therefore, we treated MDA-MB231 3D spheroids with 1 μ M BMS777607 and 5 μ M lapatinib and assessed their viability under starving conditions (0% FBS). Cell viability was significantly reduced up to 50% by a combination of 1 μ M BMS777607 and 5 μ M lapatinib compared to the effect of either inhibitor administered alone (Figure 7A). The cell viability of Ovarc8 cell spheroids was significantly inhibited by 5 μ M lapatinib and the combination of 1 μ M BMS777607 and 5 μ M lapatinib. The cell viability was inhibited to 56% by the combination of 1 μ M BMS777607 and 5 μ M lapatinib (Figure 7B).

The images of Figure 7, C and D, visualize the spheroids formed after 72 hours in Matrigel. Ovarc8 cell spheroids react more sensitively to 5 μ M lapatinib treatment alone due to the fact of higher HER2 expression levels and resulting dependency on HER2 signaling.

Analogous but less pronounced results were achieved with MDA-MB231 3D spheroids cultured under full-serum conditions (10% FBS). The cell viability of MDA-MB231 spheroids decreased significantly under full-serum conditions by combination treatment with 1 μ M BMS777607 and 5 μ M lapatinib. To better present the differences in cell viability, we displayed the inhibition of cell viability in Figure 7, E and F. The cell viability of MDA-MB231 3D spheroids was not significantly affected by 1 μ M BMS777607 or 5 μ M lapatinib alone, whereas MDA-MB231 3D spheroids treated with the TKI combination displayed a statistically significant reduction in viability of 24% (Figure 7E). To underline the efficacy of combined targeted therapies toward Axl and HER3, we performed siRNA experiments to knockdown Axl and HER3 (Figure 7F). Analogous to the pharmacological inhibition, the cell viability of MDA-MB231 3D spheroids was not significantly affected by Axl

Figure 7. Pharmacological inhibition of Axl sensitizes for lapatinib. (A) BMS777607 and lapatinib exhibit a synergistic effect on inhibition of cell viability. Cell viability of MDA-MB231 cells was measured by CellTiter-Glo assay after 72 hours of treatment. MDA-MB231 3D spheroids were incubated with 1 μ M BMS777607, 5 μ M lapatinib, or a combination of both compounds relative to DMSO control under starving conditions (0% FBS). Cell viability was reduced to 49.5% by the combination of 5 μ M lapatinib and 1 μ M BMS777607 compared to either compound administered separately. Mean values and SEM of three independent experiments are shown. Differences with $*P < .05$, $**P < .01$, and $***P < .001$ were considered statistically significant (Kruskal-Wallis test; ns, nonsignificant). (B) BMS777607 and lapatinib exhibit an additive cell viability inhibition effect. Cell viability of Ovarc8 cells was measured by CellTiter-Glo assay after 72 hours of treatment. Ovarc8 3D spheroids were incubated with 1 μ M BMS777607, 5 μ M lapatinib, or a combination of both compounds relative to DMSO control under starving conditions (0% FBS). Cell viability was reduced to 56% by the combination of 5 μ M lapatinib and 1 μ M BMS777607 compared to either compound administered separately. Mean values and SEM of three independent experiments are shown. Differences with $*P < .05$, $**P < .01$, and $***P < .001$ were considered statistically significant (Kruskal-Wallis test; ns, nonsignificant). (C) Representative phase-contrast images of MDA-MB231 spheroids. MDA-MB231 3D spheroids were incubated with 1 μ M BMS777607, 5 μ M lapatinib, or a combination of both compounds relative to DMSO control under starving conditions (0% FBS) for 72 hours. Scale bars indicate 100 μ m. (D) Representative phase-contrast images of Ovarc8 spheroids. Ovarc8 spheroids were incubated with 1 μ M BMS777607, 5 μ M lapatinib, or a combination of both compounds relative to DMSO control under starving conditions (0% FBS) for 72 hours. Scale bars indicate 100 μ m. (E) Validation of the synergistic inhibitory effect of BMS777607 and lapatinib treatment on cell viability. Cell viability of MDA-MB231 cells was measured by CellTiter-Glo assay after 72 hours of treatment. MDA-MB231 3D spheroids were incubated with 1 μ M BMS777607, 5 μ M lapatinib, or a combination of both compounds relative to DMSO control under full-serum conditions (10% FBS). Inhibition of cell viability was significantly increased to 24% by a combination of 5 μ M lapatinib and 1 μ M BMS777607 compared to either compound administered separately. Mean values and SEM of six independent experiments are shown. Differences with $*P < .05$, $**P < .01$, and $***P < .001$ were considered statistically significant (Kruskal-Wallis test; ns, nonsignificant). (F) Validation of synergistic inhibitory effect by knockdown of Axl and HER3 on cell viability. MDA-MB231 cell were transfected with Axl-specific siRNA, HER3-specific siRNA, or a combination of both siRNAs for 48 hours. Subsequently, MDA-MB231 3D spheroids were grown for 72 hours under full-serum conditions (10% FBS), and cell viability was measured by CellTiter-Glo assay. Inhibition of cell viability was significantly increased to 22% by a combination of Axl-specific siRNA and HER3-specific siRNA compared to either siRNA transfected separately. Mean values and SEM of five independent experiments are shown. Differences with $*P < .05$, $**P < .01$, and $***P < .001$ were considered statistically significant (Kruskal-Wallis test; ns, nonsignificant).

siRNA or HER3 siRNA, whereas MDA-MB231 3D spheroids treated with a combination of these two siRNAs displayed a statistically significant reduction in viability of 22% (Figure 7F).

These data suggest that pharmacological inhibition of Axl may not be an effective single-agent therapy in Axl-expressing tumors, whereas the simultaneous blockade of Axl and HER2/3 complexes at the cell surface using lapatinib might be a suitable approach to optimize the antitumor action of inhibitors targeting the Axl RTK.

Discussion

The benefits of single-target therapies are limited due to resistance formation by the activation of alternative RTKs [38]. Understanding the reasons for the acquired resistance would be an important key to a more successful cancer therapy. Hence, we asked whether targeted Axl therapies would also result in the activation of alternative RTKs. In this study, we show for the first time, that on knockdown of Axl expression by siRNA or pharmacological inhibition with BMS777607 and R428, MDA-MB231 and Ovar8 cells are able to compensate the loss of Axl activity by the induction of HER3 phosphorylation.

Furthermore, the analysis of 20 Axl-expressing cell lines from brain, breast, ovary, cervix, lung, and pancreatic cancer provided the first evidence for a positive correlation between a low basal phosphorylation of AKT S473 and the induction of HER3 activation on Axl inhibition by BMS777607 or Axl-specific siRNA-mediated knockdown. Accordingly, 7 of 10 cell lines with low pAKT S473 basal levels activated pHER3 Y1289 on treatment with BMS777607 or Axl-specific siRNA-mediated knockdown. In contrast, only 2 of 10 cell lines with high pAKT S473 basal levels showed phosphorylation of HER3 Y1289 on Axl inhibition or knockdown (Figure 3C). The high basal phosphorylation of AKT S473 mainly appears in cell lines with loss of PTEN- or PI3K-activating mutations such as the brain tumor cell lines U373, SF126, and U118 [39,40]. These cell lines are less sensitive to the Axl/PI3K/AKT signaling pathway inhibition and do not respond through HER3 up-regulation to the inhibition of the upstream RTK Axl. We conclude that inhibition of Axl induces the phosphorylation of HER3, and this induction is not confined to a particular type of tumor but is restricted to tumors with low basal activation of AKT. We suppose that AKT phosphorylation is the key sensor for upstream signaling pathways. Thus, we reason that high AKT phosphorylation levels, resulting from PTEN loss, PI3K activating mutations, or manifold affecting upstream pathways (RTKs, G-protein coupled receptors (GPCRs), integrins, and cytosolic kinases), reduce the sensitivity of the AKT sensor to upstream RTK inhibition. *Vice versa*, low basal AKT phosphorylation levels indicate a higher sensitivity of the AKT sensor to upstream RTK inhibition. Axl was shown to influence AKT phosphorylation significantly as reviewed by Verma et al., 2011 and Pazzes et al., 2014 [7,41]. In the case of Axl-overexpressing cells, as used in the present study, this correlates with higher dependency on the upstream Axl-RTK signaling pathway.

Consequently, we assume that the levels of pAKT S473 and pHER3 could be suitable biomarkers for Axl therapy response, indicating potential clinical use. The induction of HER3 phosphorylation could be used to discriminate between responder *versus* nonresponder patient cohorts as a pharmacodynamic biomarker monitoring therapy response. Additionally, our results indicate that patient cohorts with expression of Axl and low basal activity of AKT might benefit from a treatment with Axl inhibitors due to high dependency on the Axl/PI3K/AKT signaling pathway. To our knowledge, this is the first description of an independent biomarker for Axl treatment regimens.

A comparison of BMS777607 with R428 and with an Axl inhibitor discovered by our group, namely, MPCD84111, indicates that only MPCD84111 was able to block the HER3 phosphorylation feedback loop efficiently (Figure 1B). As a common characteristic, all three inhibitors efficiently block AKT phosphorylation. AKT has been shown to phosphorylate the FoxO family of transcription factors and thereby prevents their function [32]. Thus, we assume that AKT regulates the expression of HER3 by inhibiting FoxO-dependent transcription downstream of the Axl RTK. These results would be in line with observations of Chandralapaty et al., 2011 and Chakrabarty et al., 2012 using AKT or PI3K inhibitors to induce expression of HER3 in various tumor cell lines [30,31].

Our experiments with BMS777607 and MPCD84111 revealed that only MPCD84111 was able to block phosphorylation of HER3 completely, although the transcriptional feedback loop was induced in a similar extent to BMS777607 treatment (Figure 1B). As it is widely accepted that HER3 has an impaired kinase activity, activation of the HER3 RTK occurs only after its dimerization with other RTKs such as HER2 or EGFR [33,28]. On the basis of the knowledge that MPCD84111 targets HER2 (Figure 1D), a potential dimerization partner for HER3, we focused primarily on the HER family of RTKs. Although MDA-MB231 cells display a prototype of triple-negative breast cancer cell lines, characterized by a low HER2 expression, our study provides a line of arguments that HER2 is the essential dimerization partner for HER3. The inhibition of HER2/3 heterocomplexes has been demonstrated in two independent ways. First, in contrast to BMS777607 [24], MPCD84111 potentially inhibits HER2, as demonstrated by kinase selectivity profiling (Figure 1D). The HER2 inhibition capability of MPCD84111 was also proven in HER2-expressing MCF7 breast cancer cells (Figure 5A). Second, our results clearly demonstrate that Herceptin as well as lapatinib, two U.S. Food and Drug Administration-approved therapeutics for treatment of HER2-amplified breast cancer, are able to inhibit phosphorylation of HER3 (Figure 5B). Particularly, the inhibition of HER3 phosphorylation by Herceptin, a humanized IgG1 monoclonal antibody raised against HER2, is worth to be emphasized. For the sake of completeness, it is essential to mention that Herceptin- as well as HER2-specific knockdown could not prohibit HER3 phosphorylation totally. The complete inhibition of HER3 phosphorylation, comparable to HER3-specific knockdown, was only achieved by lapatinib, a dual-specific EGFR/HER2 TKI [42], or a combination of EGFR and HER2-specific siRNA. Therefore, we cannot exclude a partial impact of EGFR in the maintenance of HER3 phosphorylation in MDA-MB231 cells. However, EGFR-specific knockdown as well as EGFR inhibition by Erbitux and erlotinib (data not shown for erlotinib) did not interfere with HER3 phosphorylation in MDA-MB231 cells. Consequently, the dual-specific EGFR/HER2 TKI lapatinib emerged as the most efficient strategy to prohibit HER3 phosphorylation.

To our knowledge, this is the first study that supports the significant role of HER2 in maintaining the phosphorylation of HER3 in MDA-MB231 cells although its quantities are hardly detectable with the common immunoprecipitation or Western blot analysis techniques (Figure 5, C–E).

We could also support our hypothesis of the NRG1/HER2/HER3 compensation mechanism by rescue experiments in combination with cell viability assays in MDA-MB231 cells. Addition of the HER3 ligand NRG1 completely compensated the inhibitory effect of BMS777607 on cell viability, whereas proliferation was not

stimulated by NRG1 in untreated cells (Figure 6A). Our results implicate that up-regulation of HER3 expression by inhibition of the Axl/PI3K/AKT pathway is a prerequisite for NRG1 ligand-dependent activation of HER3 that might be important in the context of the tumor microenvironment and paracrine resistance to TKIs. The paracrine resistance is a common mechanism and has been described recently in patients with chronic myeloid leukemia treated with BCR-ABL kinase inhibitors as well as in patients with non-small cell lung cancer treated with EGFR inhibitors [43]. Wang et al., 2009 reported that hepatocyte growth factor (HGF) released by stromal fibroblasts induced resistance to EGFR inhibitors in non-small cell lung cancer due to Met activation [44]. A tumor-supportive role for macrophages was described by Vlaicu et al., 2013, where tumor-associated macrophages supply tumor cells with EGFR ligands [45]. The expression and secretion of NRG1 has been demonstrated for various components of the tumor environment, namely, fibroblasts, endothelial cells, and peripheral monocytes, additionally supporting the role of NRG1 in a paracrine tumor microenvironment-driven resistance mechanism *in vivo*. The expression of NRG1 in fibroblasts has been described by Wen et al., 1992 and Nagata et al., 2006 [46,47]. Cote et al., 2005 and Hedhi et al., 2011 nicely described the paracrine function of NRG1 produced by endothelial cells on cardiac myocytes [48,49]. Another *in vivo* study focused on mesenchyme-derived NRG1 regulating the epithelial morphogenesis of mouse embryonic submandibular glands [50]. The activation of human monocyticlike THP-1 [THP1] (ATCC® TIB-202™) cells and peripheral blood monocytes was accompanied by up-regulation and secretion of NRG1, leading to paracrine activation of the erb receptors and contribution to the epithelial and connective tissue proliferation [51]. The paracrine NRG1/HER3 signal initiated by bone marrow-derived mesenchymal stem cells and tumor-associated mesenchymal cells was shown to promote colorectal cancer cell progression and high NRG1 expression and was associated with poor prognosis as shown by De Boeck et al., 2013 [52]. Additionally, human blood serum contains considerable amounts of NRG1 in nanogram-per-milliliter concentration range [53]. Lately, NRG1 produced by breast tumor-initiating cells was shown to promote their proliferation and self-renewal in HER2 low-expressing tumors, including triple-negative breast tumors [54]. Our results indicate that MDA-MB231 cells secrete NRG1 in autocrine manner and that HER3 phosphorylation strongly correlates with the consumption of NRG1 after Axl inhibitor treatment (Figure 4D). *In vivo*, an additionally paracrine mechanism of tumor microenvironment-driven resistance might be considered for the NRG1 and HER3; however, this needs further investigation. The compensatory up-regulation of HER3 expression and the maintenance of HER3 phosphorylation on inhibition of Axl suggested that a combined inhibition of Axl and HER3 would synergistically inhibit tumor cell viability. Cell viability was significantly reduced by a combination of 1 μ M BMS777607 and 5 μ M lapatinib compared to single-inhibitor treatments (Figure 7, A and E). The efficacy of combined therapies targeting Axl and HER2/3 was underlined by siRNA-mediated knockdown of Axl and HER3 (Figure 7F). Analogous to the pharmacological intervention, we achieved a significant synergistic inhibition of cell viability by a combined application of both siRNAs. Together, these data suggest that, although pharmacological inhibition of Axl may not be an effective single-agent therapy in Axl-expressing cells with low basal AKT levels, blockade of HER2/3 complexes using lapatinib might be an effective approach to block the

HER3-activating feedback loop induced by Axl TKI treatment. We assume that a monotherapy with Axl inhibitors might have limited clinical activity due to a HER3 bypass mechanism. In cells that exhibit low expression of HER2/3, up-regulation and phosphorylation of HER3 are relevant mechanisms to counteract inhibition of the Axl/PI3K/AKT pathway. Consequently, Axl inhibitors should be used in combination with HER2/3 antagonists in Axl-positive tumors with low basal AKT phosphorylation or with an autocrine NRG1 loop. Therefore, alternatively to BMS777607 or R428, using MPCD84111 as an Axl inhibitor, with the capacity to block the HER2/3 bypass mechanism by direct inhibition of HER2, would be beneficial for cancer treatment. The final decision about using an Axl/HER2-selective compound, e.g., MPCD84111 or an alternative strategy of Axl inhibitors in combination with HER2/3 antagonistic agents, will of course require additional investigation in preclinical and clinical trials.

Acknowledgments

We thank Stefano Iacobelli (Department of Oncology and Experimental Medicine, University Foundation 'G D'Annunzio' Chieti-Pescara) for providing the MDA-MB231 cell line and U3 Pharma for providing the Hs578T cell line. We also thank Lead Discovery Center GmbH (LCD, Dortmund, Germany) for providing the BMS777607 and R428 Axl TKIs and Gregor Kirfel (Institute for Cell Biology, University of Bonn) for critical reading of the manuscript.

References

- [1] O'Bryan JP, Frye RA, Cogswell PC, Neubauer A, Kitch B, Prokop C, Espinosa III R, Le Beau MM, Earp HS, and Liu ET (1991). *axl*, a transforming gene isolated from primary human myeloid leukemia cells, encodes a novel receptor tyrosine kinase. *Mol Cell Biol* **11**, 5016–5031.
- [2] Janssen JW, Schulz AS, Steenvoorden AC, Schmidberger M, Strehl S, Ambros PF, and Bartram CR (1991). A novel putative tyrosine kinase receptor with oncogenic potential. *Oncogene* **6**, 2113–2120.
- [3] Stitt TN, Conn G, Gore M, Lai C, Bruno J, Radziejewski C, Mattsson K, Fisher J, Gies DR, and Jones PF, et al. (1995). The anticoagulation factor protein S and its relative, Gas6, are ligands for the Tyro 3/Axl family of receptor tyrosine kinases. *Cell* **80**, 661–670.
- [4] Varnum BC, Young C, Elliott G, Garcia A, Bartley TD, Fridell YW, Hunt RW, Trail G, Clogston C, and Toso RJ, et al. (1995). Axl receptor tyrosine kinase stimulated by the vitamin K-dependent protein encoded by growth-arrest-specific gene 6. *Nature* **373**, 623–626.
- [5] Hafizi S and Dahlbäck B (2006). Signalling and functional diversity within the Axl subfamily of receptor tyrosine kinases. *Cytokine Growth Factor Rev* **17**, 295–304.
- [6] Linger RM, Keating AK, Earp HS, and Graham DK (2008). TAM receptor tyrosine kinases: biologic functions, signaling, and potential therapeutic targeting in human cancer. *Adv Cancer Res* **100**, 35–83.
- [7] Verma A, Warner SL, Vankayalapati H, Bearss DJ, and Sharma S (2011). Targeting Axl and Mer kinases in cancer. *Mol Cancer Ther* **10**, 1763–1773.
- [8] Shieh YS, Lai CY, Kao YR, Shiah SG, Chu YW, Lee HS, and Wu CW (2005). Expression of *axl* in lung adenocarcinoma and correlation with tumor progression. *Neoplasia* **7**, 1058–1064.
- [9] Song X, Wang H, Logsdon CD, Rashid A, Fleming JB, Abbruzzese JL, Gomez HF, Evans DB, and Wang H (2011). Overexpression of receptor tyrosine kinase Axl promotes tumor cell invasion and survival in pancreatic ductal adenocarcinoma. *Cancer* **117**, 734–743.
- [10] Koorstra JB, Karikari CA, Feldmann G, Bish S, Rojas PL, Offerhaus GJ, Alvarez H, and Maitra A (2009). The Axl receptor tyrosine kinase confers an adverse prognostic influence in pancreatic cancer and represents a new therapeutic target. *Cancer Biol Ther* **8**, 618–626.
- [11] Vajkoczy P, Knyazev P, Kunkel A, Capelle HH, Behrnt S, von Tengg-Kobligk H, Kiessling F, Eichelsbacher U, Essig M, and Read TA, et al. (2006). Dominant-negative inhibition of the Axl receptor tyrosine kinase suppresses brain tumor cell growth and invasion and prolongs survival. *Proc Natl Acad Sci U S A* **103**, 5799–5804.

- [12] Chen PX, Li QY, and Yang Z (2013). Axl and prostasin are biomarkers for prognosis of ovarian adenocarcinoma. *Ann Diagn Pathol* **17**, 425–429.
- [13] Byers LA, Diao L, Wang J, Saintigny P, Girard L, Peyton M, Shen L, Fan Y, Giri U, and Tumula PK, et al. (2013). An epithelial–mesenchymal transition gene signature predicts resistance to EGFR and PI3K inhibitors and identifies Axl as a therapeutic target for overcoming EGFR inhibitor resistance. *Clin Cancer Res* **19**, 279–290.
- [14] Gjerdum C, Tiron C, Høiby T, Stefansson I, Haugen H, Sandal T, Collett K, Li S, McCormack E, and Gjertsen BT, et al. (2010). Axl is an essential epithelial-to-mesenchymal transition-induced regulator of breast cancer metastasis and patient survival. *Proc Natl Acad Sci U S A* **107**, 1124–1129.
- [15] Gustafsson A, Martuszewska D, Johansson M, Ekman C, Hafizi S, Ljungberg B, and Dahlbäck B (2009). Differential expression of Axl and Gas6 in renal cell carcinoma reflecting tumor advancement and survival. *Clin Cancer Res* **15**, 4742–4749.
- [16] Hutterer M, Knyazev P, Abate A, Reschke M, Maier H, Stefanova N, Knyazeva T, Barbieri V, Reindl M, and Muigg A, et al. (2008). Axl and growth arrest–specific gene 6 are frequently overexpressed in human gliomas and predict poor prognosis in patients with glioblastoma multiforme. *Clin Cancer Res* **14**, 130–138.
- [17] Rochlitz C, Lohri A, Bacchi M, Schmidt M, Nagel S, Fopp M, Fey MF, Herrmann R, and Neubauer A (1999). Axl expression is associated with adverse prognosis and with expression of Bcl-2 and CD34 in *de novo* acute myeloid leukemia (AML): results from a multicenter trial of the Swiss Group for Clinical Cancer Research (SAKK). *Leukemia* **13**, 1352–1358.
- [18] Macleod K, Mullen P, Sewell J, Rabiasz G, Lawrie S, Miller E, Smyth JF, and Langdon SP (2005). Altered ErbB receptor signaling and gene expression in cisplatin-resistant ovarian cancer. *Cancer Res* **65**, 6789–6800.
- [19] Hong CC, Lay JD, Huang JS, Cheng AL, Tang JL, Lin MT, Lai GM, and Chuang SE (2008). Receptor tyrosine kinase AXL is induced by chemotherapy drugs and overexpression of AXL confers drug resistance in acute myeloid leukemia. *Cancer Lett* **268**, 314–324.
- [20] Liu L, Greger J, Shi H, Liu Y, Greshock J, Annan R, Halsey W, Sathe GM, Martin AM, and Gilmer TM (2009). Novel mechanism of lapatinib resistance in HER2-positive breast tumor cells: activation of AXL. *Cancer Res* **69**, 6871–6878.
- [21] Mahadevan D, Cooke L, Riley C, Swart R, Simons B, Della Croce K, Wisner L, Iorio M, Shakalya K, and Gawarek H, et al. (2007). A novel tyrosine kinase switch is a mechanism of imatinib resistance in gastrointestinal stromal tumors. *Oncogene* **26**, 3909–3919.
- [22] Dufes M, Jaquel A, Belhacene N, Robert G, Cluzeau T, Luciano F, Cassuto JP, Raynaud S, and Auberger P (2011). Mechanisms of AXL overexpression and function in Imatinib-resistant chronic myeloid leukemia cells. *Oncotarget* **2**, 874–885.
- [23] Zhang Z, Lee JC, Lin L, Olivias V, Au V, Laframboise T, Abdel-Rahman M, Wang X, Levine AD, and Rho JK, et al. (2012). Activation of the AXL kinase causes resistance to EGFR-targeted therapy in lung cancer. *Nat Genet* **44**, 852–860.
- [24] Schroeder GM, An Y, Cai ZW, Chen XT, Clark C, Cornelius LA, Dai J, Gullo-Brown J, Gupta A, and Henley B, et al. (2009). Discovery of *N*-(4-(2-amino-3-chloropyridin-4-ylloxy)-3-fluorophenyl)-4-ethoxy-1-(4-fluorophenyl)-2-oxo-1,2-dihydropyridine-3-carboxamide (BMS-777607), a selective and orally efficacious inhibitor of the Met kinase superfamily. *J Med Chem* **52**, 1251–1254.
- [25] Holland SJ, Pan A, Franci C, Hu Y, Chang B, Li W, Duan M, Torneros A, Yu J, and Heckrodt TJ, et al. (2010). R428, a selective small molecule inhibitor of Axl kinase, blocks tumor spread and prolongs survival in models of metastatic breast cancer. *Cancer Res* **70**, 1544–1554.
- [26] Li Y, Ye X, Tan C, Hongo JA, Zha J, Liu J, Kallop D, Ludlam MJ, and Pei L (2009). Axl as a potential therapeutic target in cancer: role of Axl in tumor growth, metastasis and angiogenesis. *Oncogene* **28**, 3442–3455.
- [27] Mackiewicz M, Huppi K, Pitt JJ, Dorsey TH, Ambs S, and Caplen NJ (2011). Identification of the receptor tyrosine kinase AXL in breast cancer as a target for the human miR-34a microRNA. *Breast Cancer Res Treat* **130**, 663–679.
- [28] Campbell MR, Amin D, and Moasser MM (2010). HER3 comes of age: new insights into its functions and role in signaling, tumor biology, and cancer therapy. *Clin Cancer Res* **16**, 1373–1383.
- [29] Révillion F, Lhotellier V, Hornez L, Bonnetterre J, and Peyrat JP (2008). *ErbB/HER* ligands in human breast cancer, and relationships with their receptors, the bio-pathological features and prognosis. *Ann Oncol* **19**, 73–80.
- [30] Chandralapaty S, Sawai A, Scaltriti M, Rodrik-Outmezguine V, Grbovic-Huezo O, Serra V, Majumder PK, Baselga J, and Rosen N (2011). AKT inhibition relieves feedback suppression of receptor tyrosine kinase expression and activity. *Cancer Cell* **19**, 58–71.
- [31] Chakrabarty A, Sánchez V, Kuba MG, Rinehart C, and Arteaga CL (2012). Feedback upregulation of HER3 (ErbB3) expression and activity attenuates antitumor effect of PI3K inhibitors. *Proc Natl Acad Sci U S A* **109**, 2718–2723.
- [32] Myatt SS and Lam EW (2007). The emerging roles of forkhead box (Fox) proteins in cancer. *Nat Rev Cancer* **7**, 847–859.
- [33] Hynes NE and Lane HA (2005). ERBB receptors and cancer: the complexity of targeted inhibitors. *Nat Rev Cancer* **5**, 341–354.
- [34] Stern DF (2008). ERBB3/HER3 and ERBB2/HER2 duet in mammary development and breast cancer. *J Mammary Gland Biol Neoplasia* **13**, 215–223.
- [35] Blobel CP (2005). ADAMs: key components in EGFR signalling and development. *Nat Rev Mol Cell Biol* **6**, 32–43.
- [36] Borrell-Pagès M, Rojo F, Albanell J, Baselga J, and Arribas J (2003). TACE is required for the activation of the EGFR by TGF- α in tumors. *EMBO J* **22**, 1114–1124.
- [37] Dong J, Opreko LK, Dempsey PJ, Lauffenburger DA, Coffey RJ, and Wiley HS (1999). Metalloprotease-mediated ligand release regulates autocrine signaling through the epidermal growth factor receptor. *Proc Natl Acad Sci U S A* **96**, 6235–6240.
- [38] Engelman JA and Settleman J (2008). Acquired resistance to tyrosine kinase inhibitors during cancer therapy. *Curr Opin Genet Dev* **18**, 73–79.
- [39] Parsa AT, Waldron JS, Panner A, Crane CA, Parney IF, Barry JJ, Cachola KE, Murray JC, Tihan T, and Jensen MC, et al. (2007). Loss of tumor suppressor PTEN function increases B7-H1 expression and immunoresistance in glioma. *Nat Med* **13**, 84–88.
- [40] Eitel JA, Bijangi-Vishehsaraei K, Saadatzadeh MR, Bhavsar JR, Murphy MP, Pollok KE, and Mayo LD (2009). PTEN and p53 are required for hypoxia induced expression of maspin in glioblastoma cells. *Cell Cycle* **8**, 896–901.
- [41] Paccet JD, Vogelsang M, Parker MI, and Zerbini LF (2014). The receptor tyrosine kinase Axl in cancer: biological functions and therapeutic implications. *Int J Cancer* **134**, 1024–1033.
- [42] Davis MI, Hunt JP, Herrgard S, Ciceri P, Wodicka LM, Pallares G, Hocker M, Treiber DK, and Zarrinkar PP (2011). Comprehensive analysis of kinase inhibitor selectivity. *Nat Biotechnol* **29**, 1046–1051.
- [43] Hölzel M, Bovier A, and Tüting T (2013). Plasticity of tumour and immune cells: a source of heterogeneity and a cause for therapy resistance? *Nat Rev Cancer* **13**, 365–376.
- [44] Wang W, Li Q, Yamada T, Matsumoto K, Matsumoto I, Oda M, Watanabe G, Kayano Y, Nishioka Y, and Sone S, et al. (2009). Crosstalk to stromal fibroblasts induces resistance of lung cancer to epidermal growth factor receptor tyrosine kinase inhibitors. *Clin Cancer Res* **15**, 6630–6638.
- [45] Vlaicu P, Mertins P, Mayr T, Widschwendter P, Ataseven B, Högel B, Eiermann W, Knyazev P, and Ullrich A (2013). Monocytes/macrophages support mammary tumor invasivity by co-secreting lineage-specific EGFR ligands and a STAT3 activator. *BMC Cancer* **13**, 197.
- [46] Wen D, Peles E, Cupples R, Suggs SV, Bacus SS, Luo Y, Trail G, Hu S, Silbiger SM, and Levy RB, et al. (1992). Neu differentiation factor: a transmembrane glycoprotein containing an EGF domain and an immunoglobulin homology unit. *Cell* **69**, 559–572.
- [47] Nagata K, Wada K, Tatsuguchi A, Futagami S, Gudis K, Miyake K, Tsukui T, and Sakamoto C (2006). Heregulin- α and heregulin- β expression is linked to a COX-2-PGE2 pathway in human gastric fibroblasts. *Am J Physiol Gastrointest Liver Physiol* **290**, G1243–G1251.
- [48] Cote GM, Miller TA, Lebrasseur NK, Kuramochi Y, and Sawyer DB (2005). Neuregulin-1 α and β isoform expression in cardiac microvascular endothelial cells and function in cardiac myocytes *in vitro*. *Exp Cell Res* **311**, 135–146.
- [49] Hedhli N, Huang Q, Kalinowski A, Palmeri M, Hu X, Russell RR, and Russell KS (2011). Endothelium-derived neuregulin protects the heart against ischemic injury. *Circulation* **123**, 2254–2262.
- [50] Miyazaki Y, Nakanishi Y, and Hieda Y (2004). Tissue interaction mediated by neuregulin-1 and ErbB receptors regulates epithelial morphogenesis of mouse embryonic submandibular gland. *Dev Dyn* **230**, 591–596.
- [51] Mograbi B, Rochet N, Imbert V, Bourget I, Bocciarelli R, Emiliozzi C, and Rossi B (1997). Human monocytes express amphiregulin and heregulin growth factors upon activation European cytokine network. *Eur Cytokine Netw* **8**, 73–81.
- [52] De Boeck A, Pauwels P, Hensen K, Rummens JL, Westbroek W, Hendrix A, Maynard D, Denys H, Lambain K, and Braems G, et al. (2013). Bone marrow-derived mesenchymal stem cells promote colorectal cancer progression through paracrine neuregulin 1/HER3 signalling. *Gut* **62**, 550–560.
- [53] Shibuya M, Komi E, Wang R, Kato T, Watanabe Y, Sakai M, Ozaki M, Someya T, and Nawa H (2010). Measurement and comparison of serum neuregulin 1 immunoreactivity in control subjects and patients with schizophrenia: an influence of its genetic polymorphism. *J Neural Transm* **117**, 887–895.
- [54] Lee CY, Lin Y, Bratman S, Feng W, Kuo A, Scheeren F, Engreitz JM, Varma S, West R, and Diehn M (2013). Neuregulin autocrine signaling promotes self-renewal of breast tumor-initiating cells by triggering HER2/HER3 activation. *Cancer Res* **74**, 341–352.